Neuroscience 2011

# SHORT COURSE III

## BACs, TRAPs, and Targeted Mutations:
Revealing Secrets of the Mammalian Brain Using Advanced Genetic Approaches

Organized by Nathaniel Heintz, PhD

SOCIETY FOR NEUROSCIENCE

# Short Course III

## BACs, TRAPs, and Targeted Mutations: Revealing Secrets of the Mammalian Brain Using Advanced Genetic Approaches

Organized by Nathaniel Heintz, PhD

SOCIETY FOR NEUROSCIENCE

Please cite articles using the model:

[AUTHOR'S LAST NAME, AUTHOR'S FIRST & MIDDLE INITIALS] (2011)
[CHAPTER TITLE] In: BACs, TRAPs, and Targeted Mutations: Revealing Secrets of the
Mammalian Brain Using Advanced Genetic Approaches.
(Heintz N, ed) pp. [xx-xx]. Washington, DC: Society for Neuroscience.

# Table of Contents

# Introduction

Although classical histological studies established that the morphology of specific neural cell types in the mammalian brain varies dramatically, the ability to genetically target these cell types and understand the biochemical basis of their structure and function eluded scientists for nearly a century. To address this problem, a variety of novel approaches have been developed for the investigation of genes, cells, and circuits *in vivo*. This day-long course consists of a series of lectures by the faculty illustrating the power of cell-specific genetic strategies for investigation of mechanisms that contribute to the histological and functional complexities of the mammalian brain, followed by informal breakout sessions, and includes a syllabus book.

Course Organizer: Nathaniel Heintz, PhD, Rockefeller University, Howard Hughes Medical Institute. Faculty: David D. Ginty, PhD, Department of Neuroscience, Johns Hopkins University School of Medicine; Stephen Hitchcock, PhD, Envoy Therapeutics; Ines Ibanez-Tallon, PhD, Department of Molecular Neurobiology, Max-Delbrück Center for Molecular Medicine, Berlin; Botond Roska, PhD, MD, Neural Circuit Laboratories, Friedrich Miescher Institute for Biomedical Research; Fekrije Selimi, PhD, Center for Interdisciplinary Research in Biology, Collège de France; Huda Y. Zoghbi, MD, Baylor College of Medicine, Howard Hughes Medical Institute, Jan and Dan Duncan Neurological Research Institute.

# Considerations for Target Selection in CNS Drug Discovery Programs

Stephen A. Hitchcock, PhD

Envoy Therapeutics
Jupiter, Florida

NOTES

## The Druggable Genome

Currently approved drugs mediate their therapeutic effects via a relatively small subpopulation of the druggable genome. Contemporary estimates suggest that approximately 3000 druggable genes exist, yet current drugs act on only ~400 defined unique molecular targets (Rask-Andersen et al., 2011). These statistics suggest that the vast majority of the druggable genome is, as yet, unexploited by pharmacotherapy. The current repertoire of drugged targets is dominated by cell surface receptors, transporters, and soluble enzymes (Fig. 1). The drugged members within these target families are considered by many to represent the "low-hanging fruit" within the druggable genome, implying that the next generation of targets will be substantially more challenging.

The concept of small-molecule druggability has evolved from an analysis of the overlap between druggable biological target space and oral drug-like chemical space. The convergence of these two concepts requires first that the target play a role in human disease and second that it has the potential to be modulated in a selective manner by a small molecule that has oral, drug-like physicochemical properties. A target's druggability is usually estimated by classifying it with known gene families that have previously been successfully targeted with drugs. However, this approach has some inherent limitations, so for targets of known structure, researchers have used a mathematical model that uses structural information about a target's binding site in order to estimate a maximal achievable affinity for a drug-like molecule (Cheng et al., 2007).

The concept of oral drug-likeness has its origins in the mid 1990s and initially centered on the relationship between compound properties and solubility and permeability. The Lipinski Rule of Five (Lipinski, 2004) provided guidelines for oral drug-likeness based on lipophilicity, as defined by the logarithm of the octanol/water partition coefficient (logP $\leqslant$ 5), hydrogen bond donor count (HBD $\leqslant$ 5), hydrogen bond acceptor count (HBA $\leqslant$ 10), and molecular weight (MW $\leqslant$ 500 Da). Further analyses of druggable chemical space have revealed additional relationships between compound properties and other absorption, distribution, metabolism, excretion, and toxicity (ADMET) properties that must be satisfied for a successful drug candidate (Meanwell, 2011). Favorable ADMET properties and biological target potency generally show a diametrically opposed relationship with respect to MW and logP. There is also a growing body of evidence that compound promiscuity on average increases with increasing MW and logP. This characteristic suggests that the level of potency sought in a candidate molecule must be carefully balanced with physical properties, ADMET characteristics, and promiscuity — especially for CNS targets (Gleeson et al., 2011).

## The CNS Druggable Genome

Despite recent advances in technology demonstrating the delivery of antibodies across the blood–brain barrier (BBB) in animal models (Atwal et al., 2011), drugged CNS targets remain exclusively within the domain of small-molecule therapeutics. The nonfenestrated endothelium of brain capillaries that constitutes the BBB physically limits the passive permeability of compounds and presents a metabolic barrier to CNS entry in the form of metabolizing enzymes and transport proteins. A further refinement of the concept of drug-likeness is therefore required for compounds intended for CNS targets in order to account for the limitations imposed by BBB permeability. The fact that CNS-accessible chemical space represents a subset of oral drug-like space can be illustrated by plotting simple physicochemical descriptors such as MW, polar surface area (PSA), and calculated LogP (cLogP) of drugs marketed for CNS indications against those intended for peripheral targets (Fig. 2). For example, there is greater latitude for higher PSA in drugs that do not require entry into the CNS. The same is true of MW. The greater stringency around CNS compound properties translates into a

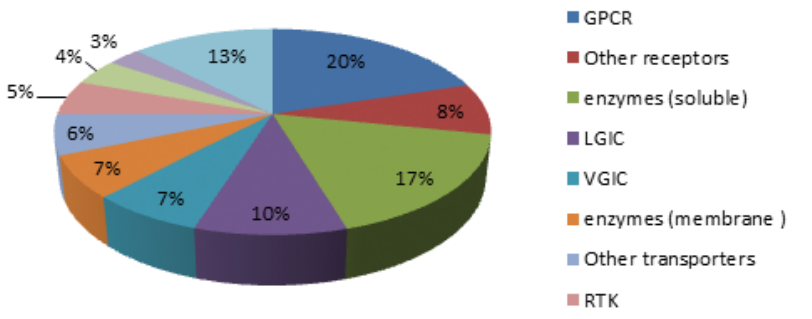


Figure 1. Percent distribution of the targets of approved therapeutics by target class (Rask-Andersen et al., 2011). LGIC, Ligand-gated ion channel; NR, nuclear receptor; RTK, receptor tyrosine kinase; SLC, solute carrier class; VGIC, Voltage-gated ion channel.

NOTES

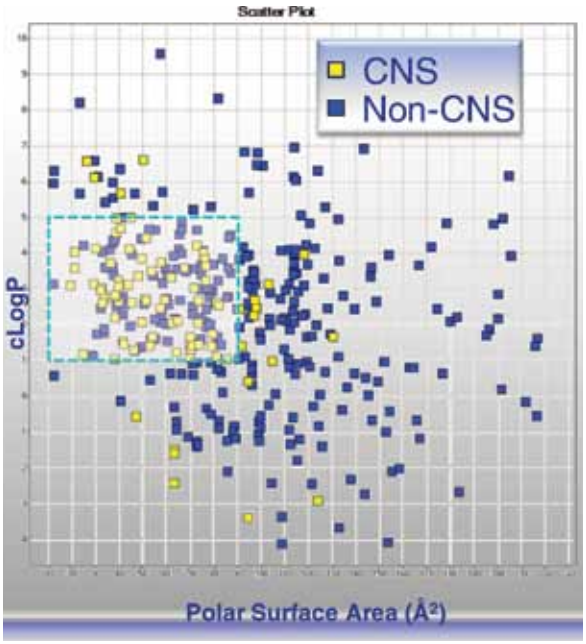


Figure 2. PSA and cLogP values of oral drugs in the MDL Drug Data Report (MDDR) database.

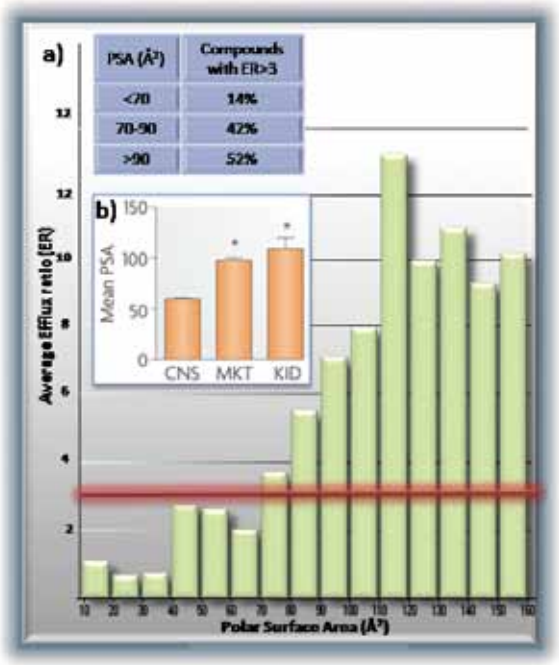


Figure 3. *a*, P-gp ER properties of 4125 compounds bucketed by PSA. *b*, Average PSA of CNS drugs, all marketed oral drugs (MKT), and kinase inhibitor drugs (KID). Chico et al. (2009), their Figure 4, adapted with permission.

lower likelihood of simultaneously achieving good BBB permeability and potent activity for targets with large and/or polar binding sites.

Retrospective analysis of marketed drugs has revealed that a very low prevalence of P-glycoprotein (P-gp) efflux, coupled with moderately to highly passive permeability, are two key properties that distinguish drugs that engage targets in the CNS from those that act predominantly in the periphery. The efflux properties that differentiate CNS drugs have been quantified using *in vitro* assays for human and rodent P-gp (Doan et al., 2002; Feng et al., 2008). Efflux properties have also been revealed *in vivo* by comparing brain drug exposures in P-gp (*mdr1a/b*$^{-/-}$) knock-out mice with those observed in wild-type mice (Doran et al., 2005). Despite the lore that correlates compound lipophilicity with brain exposure, LogP is not correlated with brain unbound drug levels, which are the true determinants of pharmacologically relevant exposure. In fact, molecular descriptors related to hydrogen bonding (PSA, HBD, HBA) dominate the relationship with the steady-state unbound brain-to-plasma concentration ratio ($K_{p,uu,brain}$) (Fridén et al., 2009). This finding likely results from the additive effect that PSA, HBD, and HBA have on simultaneously reducing passive permeability while increasing the probability of interactions with efflux transporters.

Figure 3*a* shows the relationship between PSA and average P-gp efflux ratio (ER) of 4125 compounds tested in LLC-PK cells transfected with human multidrug resistance 1 (MDR1) cDNA (P-gp). Compounds with ER >3 are considered to be P-gp substrates. Figure 3*b* illustrates the average PSA of CNS drugs, all marketed oral drugs (MKT), and kinase inhibitor drugs (KID) (Chico et al., 2009). The high PSA generally required for potent ATP-competitive kinase inhibition explains the generally poor CNS penetration of this class of compounds.

Approved CNS drugs are dominated by compounds that directly engage biogenic amine receptors or indirectly modulate their activity by inhibiting neurotransmitter metabolism or uptake. This circumstance owes much to capacity for achieving high affinity at such targets with low-molecular-weight compounds (high ligand efficiency) that have relatively low PSA and is aided by a traditionally low stringency for biological target selectivity.

The industry shift from phenotypic screening and polypharmacology to single-targeted therapeutics has been particularly hard on CNS drug discovery (Swinney and Anthony, 2011). The orthosteric binding sites among many biogenic amine G-protein coupled receptor (GPCR) family members are

highly conserved. Thus, the quest for subtype-selective ligands for even these low-hanging targets has required reliance upon additional interactions in nonconserved binding regions, thus driving up the molecular weight of compounds. The surge of interest in allosteric receptor modulators is a direct response to the challenge of attaining selectivity within the confines of CNS-accessible chemical space (Conn et al., 2009). The origins of low success rates at each stage of drug discovery are multifactorial, but the limited structural space available to achieve target engagement in the brain is a major contributing element to the high attrition in CNS programs. Despite the large industry-wide investment in new targets, only four new CNS drugs that act by previously unexploited mechanisms have been launched in the past decade in the United States (Table 1).

Table 1. CNS Drugs launched during 2000–2010 that act on new targets.

| Drug | Target | Gene family | Launch | Indication |
|---|---|---|---|---|
| Aprepitant | NK1 | GPCR | 2003 | CINV |
| Ramelteon | MT1/MT2 | GPCR | 2005 | Insomnia |
| Varenicline | α4β2 | LGIC | 2006 | Nicotine addiction |
| Fingolimod | S1P1 | GPCR | 2010 | Multiple sclerosis |

CINV, Chemotherapy-induced nausea and vomiting; GPCR, G-protein coupled receptor; LGIC, ligand-gated ion channel.

Simple physicochemical guidelines and computational models can be helpful in altering the probability of encountering P-gp efflux; however, it is abundantly evident that compounds with identical physicochemical properties can have vastly different efflux properties. As with any small molecule–protein interaction, the composition and presentation of functionality on a molecule play a critical role in the recognition process. However, unlike the typical small molecule–drug target interaction, P-gp is a highly permissive protein recognizing a wide diversity of substrates. Biological targets with larger, more polar binding sites (such as those that have peptides, amino acids, and nucleotides as ligands or substrates) are disadvantaged when it comes to achieving sufficient target affinity within physicochemical space that is favorable for CNS entry. However, this limitation does not mean that reconciling potency, selectivity, and CNS entry for such targets is impossible; it is simply more demanding.

The aspartyl protease β-amyloid cleaving enzyme-1 (BACE1) is a good example. BACE is a hotly pursued target in the quest for a disease-modifying therapy for Alzheimer's disease (Varghese, 2010). Reconciling the structural requirements for potency and protease selectivity with the need for low metabolic clearance, adequate passive permeability, and avoidance of P-gp efflux in individual compounds has proven extremely challenging for those that have tackled BACE inhibitor optimization. It is worthwhile contrasting the timeline involved in advancing HIV protease inhibitors from target discovery to drug launch with the time that has elapsed since the first disclosure of BACE as a molecular target. HIV protease was first disclosed in 1988 and, remarkably, within seven short years, saquinavir had received FDA approval and was quickly followed by several other entries. In contrast, BACE was disclosed in 1999 and only recently have the first inhibitors begun to enter clinical development, still many years from potential FDA approval. Although many factors distinguish HIV infection from Alzheimer's disease, a major differentiator is the absolute requirement that BACE inhibitors enter the CNS. The requirement for CNS penetration imparts additional confinements around available structural and physicochemical space, reducing the scope of options for solving potency, selectivity, and pharmacokinetic deficiencies.

Numerous other examples highlight successful efforts to engineer CNS target coverage while maintaining biological target activity, selectivity, and in many cases, favorable pharmacokinetic properties for targets with large and/or polar binding sites. These include bradykinin, orexin, opioid peptide GPCRs, GABA, glutamate and glycine receptors, and several phosphodiesterases and kinases.

## Target Selection and Validation

It has been said that a drug target's relevance to disease is often inferred with strong belief but fragile evidence. It can also be argued that, since the complete sequencing of the human genome, the key task in biomedical research is no longer target identification but rather target validation. However, given the additional limitations around CNS-accessible chemical space, assessment of potential targets for the probability of achieving CNS druggability should be conducted early in the target selection process. Druggability should then be weighed against other evidence in support of or against the target. Target validation is a continuum whereby an increasing

NOTES

body of data is amassed that culminates in positive efficacy in humans. The initial target selection and subsequent validation path may include evidence from the expression pattern of the target, human and animal genetics, validation in animal disease models (preferably across multiple species), and observations with model compounds (based on human or animal data). The target selection and validation path should also include consideration of a human biomarker, preferably a functional endpoint or surrogate endpoint.

In recent years, there has been a number of high-profile CNS drugs subject to black box label warnings, others subject to outright withdrawal, and FDA rejections of several CNS drug candidates. In many cases, mechanism-related side effects have resulted in an unfavorable risk-to-benefit ratio for the patient. Therefore, in addition to establishing target validation, assessing the likelihood and nature of mechanism-related side effects and the ability to empirically measure and defuse these risks early in the drug discovery process are important. Pursuing targets that have selective expression patterns (preferably limited to the dysfunctional circuit or cell type of interest) would confer the advantage of lowering the probability of mechanism-related side effects.

## References


Atwal JK, Chen Y, Chiu C, Mortensen DL, Meilandt WJ, Liu Y, Heise CE, Hoyte K, Luk W, Lu Y, Peng K, Wu P, Rouge L, Zhang Y, Lazarus RA, Scearce-Levie K, Wang W, Wu Y, Tessier-Lavigne M, Watts RJ (2011) A therapeutic antibody targeting BACE1 inhibits amyloid-β production *in vivo*. Sci Transl Med 3:84ra43.

Cheng AC, Coleman RG, Smyth KT, Cao Q, Soulard P, Caffrey DR, Salzberg AC, Huang ES (2007) Structure-based maximal affinity model predicts small-molecule druggability. Nat Biotechnol 25:71-75.

Chico LK, Van Eldik LJ, Watterson DM (2009) Targeting protein kinases in central nervous system disorders. Nat Rev Drug Discov 8:892-909.

Conn PJ, Christopoulos A, Lindsley CW (2009) Allosteric modulators of GPCRs: a novel approach for the treatment of CNS disorders. Nat Rev Drug Discov 8:41-54.

Doran A, Obach RS, Smith BJ, Hosea NA, Becker S, Callegari E, Chen C, Chen X, Choo E, Cianfrogna J, Cox LM, Gibbs JP, Gibbs MA, Hatch H, Hop CE, Kasman IN, Laperle J, Liu J, Liu X, Logman M, et al. (2005) The impact of P-glycoprotein on the disposition of drugs targeted for indications of the central nervous system: evaluation using the MDR1A/1B knockout mouse model. Drug Metab Dispos 33:165-174.

Feng B, Mills JB, Davidson RE, Mireles RJ, Janiszewski JS, Troutman MD, de Morais SM (2008) *In vitro* P-glycoprotein assays to predict the *in vivo* interactions of P-glycoprotein with drugs in the central nervous system. Drug Metab Dispos 36:268-275.

Fridén M, Winiwarter S, Jerndal G, Bengtsson O, Wan H, Bredberg U, Hammarlund-Udenaes M, Antonsson M (2009) Structure-brain exposure relationships in rat and human using a novel data set of unbound drug concentrations in brain interstitial and cerebrospinal fluids. J Med Chem 52:6233-6243.

Gleeson MP, Hersey A, Montanari D, Overington J (2011) Probing the links between *in vitro* potency, ADMET and physicochemical parameters. Nat Rev Drug Discov 10:197-208.

Lipinski CA (2004) Lead- and drug-like compounds: the rule-of-five revolution. Drug Discov Today Technol 1:337-341.

Mahar Doan KM, Humphreys JE, Webster LO, Wring SA, Shampine LJ, Serabjit-Singh CJ, Adkison KK, Polli JW (2002) Passive permeability and P-glycoprotein-mediated efflux differentiate central nervous system (CNS) and non-CNS marketed drugs. J Pharmacol Exp Ther 303:1029-1037.

Meanwell NA (2011) Improving drug candidates by design: a focus on physicochemical properties as a means of improving compound disposition and safety. Chem Res Toxicol 24:1420-1456.

Rask-Andersen M, Almén MS, Schiöth HB (2011) Trends in the exploitation of novel drug targets. Nat Rev Drug Discov 10:579-590.

Swinney DC, Anthony J (2011) How were new medicines discovered? Nat Rev Drug Discov 10:507-519.

Varghese J (2010) (Ed.) BACE: Lead target for orchestrated therapy of Alzheimer's disease. Hoboken, NJ: Wiley.

# Molecular Dissection of Neural Circuits Controlling Nicotine Aversion

Silke Frahm, PhD; Marta A. Slimak;
Julio Santos-Torres, PhD;
Beatriz Antolin-Fontes; Sebastian Auer, PhD;
and Inés Ibañez-Tallon, PhD

Department of Molecular Neurobiology
Max Delbrück Center for Molecular Medicine
Berlin, Germany

NOTES

## Introduction

Tobacco use is a major public health challenge leading to millions of preventable deaths every year (http://www.who.int/tobacco/statistics/tobacco_atlas/en/). The principal addictive component of tobacco is the plant alkaloid nicotine, which binds and activates nicotinic acetylcholine receptors (nAChRs) (Dani and Heinemann, 1996). In the mammalian nervous system, eight alpha (α2–α7 and α9–α10) and three beta (β2–β4) subunits assemble into pentameric nAChR combinations with distinctive pharmacological and functional properties (McGehee and Role, 1995; Gotti et al., 2009). Recently, genome-wide association studies (GWAS) have identified genetic variants in the *Chrnb4–CHRNA3–CHRNA5* gene cluster as risk factors for nicotine dependence and lung cancer (Thorgeirsson et al., 2008; Weiss et al., 2008; Saccone et al., 2009; Amos et al., 2010a). These single nucleotide polymorphisms (SNPs) include noncoding variants across the gene cluster, as well as amino acid substitutions (http://www.ncbi.nlm.nih.gov/snp/). Given that *cis*-regulatory elements within the cluster coordinate transcription of these genes for assembly of α3β4-containing (α3β4*) and α3β4α5 functional nAChRs (Xu et al., 2006; Scofield et al., 2010), the fact that a large number of SNPs map to noncoding segments of the cluster suggests that altered regulation of these genes can contribute to the pathophysiology of tobacco use. Indeed, the risk for nicotine dependence seems to stem from at least two separate mechanisms: the variability in the mRNA levels of these genes and functional changes due to nonsynonymous amino acid variants (Lu et al., 2009).

A number of mouse models with gene deletions, point mutations, or strain-specific variants in nAChR subunits have been critical to elucidating the role of the different nAChR combinations in nicotine addiction and withdrawal. For instance, α4β2 nAChRs (accounting for 80% of the high-affinity nicotine binding sites in the brain) (Whiting and Lindstrom, 1988) are major contributors to nicotine self-administration, as shown in β2 knock-out (KO) mice (Picciotto, 1998; Maskos et al., 2005) and in knock-in mice with a gain-of-function mutation of α4 (Tapper et al., 2004). The nAChR β4 subunit is almost always coexpressed with α3, while the auxiliary α5 subunit assembles with the α3β4 combination but can also be incorporated into α4β2 receptor complexes. The expression of the α3β4* nAChR combination is restricted to a few discrete brain areas, including the medial habenula (mHb) and interpeduncular nucleus (IPN), and to autonomic ganglia (Zoli et al., 1995). α3β4* nAChRs have a lower affinity for nicotine than α4β2 receptors and are likely less desensitized at the nicotine levels found in smokers than α4β2 nAChRs. This suggests that α3β4* nAChRs could play an important role in tobacco addiction, since they retain their sensitivity to fluctuating nicotine levels in smokers (Rose, 2007). β4 and α5 KO mice show similar phenotypes, including decreased signs of nicotine withdrawal symptoms (Jackson et al., 2008; Salas et al., 2004, 2009), hypolocomotion, and resistance to nicotine-induced seizures (Kedmi et al., 2004; Salas et al., 2004). It has been more difficult to assess the role of α3* nAChRs because KO mice die within 3 weeks after birth owing to severe bladder dysfunction (Xu et al., 1999).

Here we show that α3β4α5 nicotinic acetylcholine receptor activity *in vitro* and *in vivo* is limited by the level of *Chrnb4* expression and that the ability of the β4 subunit to increase α3β4α5 currents depends on a single, unique residue (S435). This residue maps to the intracellular vestibule of the nAChR complex adjacent to the rs16969968 SNP in *CHRNA5* (D398N), which has been linked to a high risk of developing nicotine dependence in humans. We present a novel transgenic mouse model of the *Chrnb4–Chrna3–Chrna5* gene cluster, referred to as Tabac (Transgenic a3b4a5 cluster) mice. In these mice, *Chrnb4* overexpression enhances α3β4* nAChR levels, resulting in altered nicotine consumption and nicotine-conditioned place aversion. Lentiviral vector–mediated transduction of the mHb of Tabac mice with the D398N *Chrna5* variant reversed the nicotine aversion induced by β4 overexpression. This study provides a new mouse model for nicotine dependence, demonstrates a critical role for the mHb in the circuitry controlling nicotine consumption, and elucidates novel molecular mechanisms that contribute to these phenotypes.

## Results

### The relative levels of α5 and β4 subunits strongly affect α3β4α5 nAChR currents

Recently, it has been shown that α5 competes with β4 for association with α4, and that this competition does not occur if β4 is substituted by β2 (Gahring and Rogers, 2010). The *CHRNB4–A3–A5* gene cluster regulates the co-expression of β4, α3 and α5 subunits, and SNPs in the regulatory regions of the cluster, as well as non-synonymous variants such as rs16969968 (corresponding to D398N in *CHRNA5*), associated with nicotine

NOTES

dependence (Bierut et al., 2008; Saccone et al., 2009; Beirut, 2010). Given these evidences, we were first interested in determining whether varying the relative expression levels of α3, β4, and α5 (wild type and D398N) subunits influences nicotine-evoked currents.

To measure this effect, we performed electrophysiological recordings in oocytes injected with cRNA transcripts of the different mouse subunits. In these experiments (Fig. 1), the cRNA concentration of α3 was held constant (1 ng/oocyte), whereas the concentration of β4 or β2 input cRNA varied from 1, 2, 4, 5 to 10 ng, respectively. These experiments showed that β4, but not β2, was able to increase current amplitudes in a dose-dependent manner (Fig. 1*A,B*). Next we held constant the concentrations of α3 and β4 at 1:10 and added the cRNA of α5 wild type (Wt) or the α5 D397N variant (corresponding to the human α5 variant D398N) at ratios of 1:10:1, 1:10:5 and 1:10:10 (Fig. 1*A*). We observed a significant decrease of current amplitudes at higher concentrations of α5, and this effect was significantly more pronounced with α5 D397N. These results suggest that α5 and β4 may compete for binding to α3, in line with the studies showing such competition for binding to α4 (Gahring and Rogers, 2010).

Given that overexpression of β2 with either α3 (Fig. 1*A*) or α4 (data not shown) did not increase currents, we were interested in identifying the residues differing between β4 and β2 that mediate this effect. Since the long cytoplasmic loop is the most divergent domain between nAChR subunits, and since it has been implicated in cell-surface expression and trafficking of β2 subunits (Nashmi et al., 2003; Ren et al., 2005), we generated β2–β4 chimeras exchanging either this domain, or short motifs and single residues within this domain. Replacement of the cytoplasmic loop of β2 with the corresponding sequences present in β4 (β2/β4 322–496) led to a strong increase of nicotinic currents (Fig. 1*C*). Introducing two β4-specific motifs: a serine/tyrosine rich motif (β2/+β4 382–391) and gephyrin-like binding motif (β2/+β4 401–419) into the β2 loop had no influence on current amplitudes (Fig. 1*C*).

We next performed bioinformatic analyses and singled out eight β4-specific residues (indicated as T-1 to T-8 in supplemental Fig. S1*C*) present within highly conserved motifs. Six of these residues were not further considered: T-2, T-3, T-6, and T-7 residues differ between mouse and chicken β4 subunits, which are equally potent in enhancing nicotine-evoked currents (Fig. S1*B*); T-4 residue lies within the tested motif in the β2/+β4 382–391 chimera; and residues at position T-8 have the same charge (Fig. S1*C*). The remaining two candidates, T-1 (S324 in β4 and T327 in β2) and T-7 (S435 in β4 and R431 in β2) (Fig. S1*C*), were tested by point mutagenesis in the β2 subunit backbone. The β2 T327S point mutant did not increase current, whereas replacement of β2 R431 with serine resulted in a 3.5-fold current increase (Fig. 1*C*). Furthermore, point mutation of the native S435 in the β4 subunit to the arginine residue present in β2 (β4 S435R) abolished the β4-specific activity. Thus, these data demonstrate that the distinctive ability of β4 to increase currents when overexpressed maps to a single residue (S435). This residue is both required in β4 for current increase and can confer this property to β2.


**Supplemental Figure 1.** Alignment of Chrnb4, Chrnb2, and Chrna5 protein sequences from different species reveals single differential amino acids within highly conserved regions. A custom track T β4/β2,α5 shows the differential conservation scores of β4 sequences compared with β2 and α5 (the resulting differential residues were designated T-3 and T-6-8). T β4/β2,α5 shows the differential conservation scores of β2 sequences compared to β4 and α5 (the resulting differential residues were designated T-1-2 and T-4-5). The tracks below show the global conservation and the consensus residues. Two residues of β4 (S324 and S435, green and red arrows) showing differential conservation score were selected for generation of β2- β4 chimeras shown in Figure 5*D*. HS, *Homo sapiens*; PT, *Pan troglodytes*; MM, *Mus musculus*; RN, *Rattus norvegicus*; BT, *Bos taurus*; GG, *Gallus gallus*; TM, transmembrane domain.

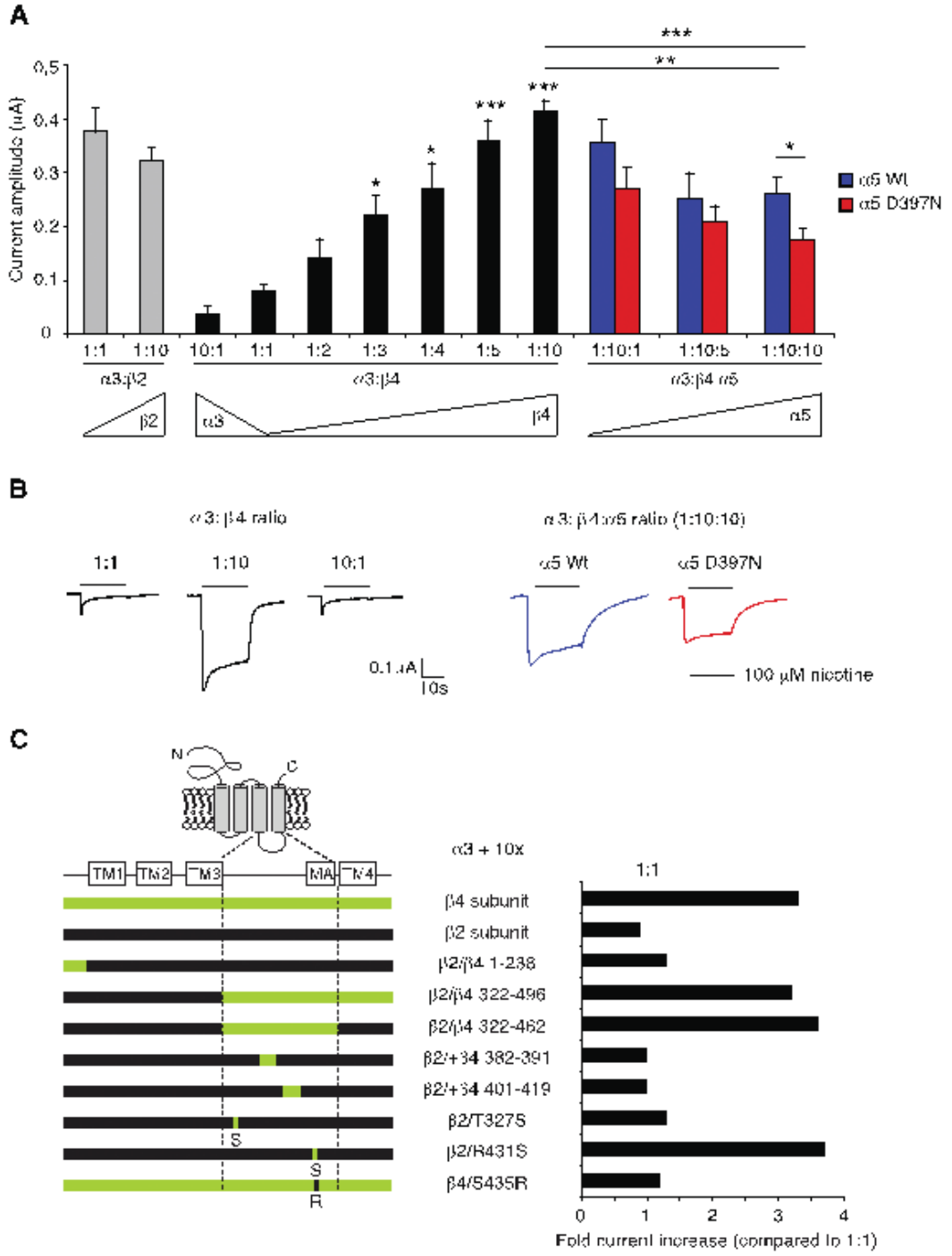


**Figure 1.** Increase of nAChR currents by β4 is competed by α5 and maps to a single amino acid (S435). ***A***, Quantification of nicotine-evoked currents (100 μM, 20 s) recorded in *Xenopus* oocytes injected with mouse α3:β2, α3:β4, and α3:β4:α5 cRNAs at the indicated ratios. Current amplitudes from 1:3 to 1:10 α3β4 combinations are significantly increased compared with 1:1 ratio (*$p < 0.05$; ***$p < 0.001$). Addition of α5 to the α3β4 complex leads to a significant decrease of current amplitudes when equal amounts of β4 and α5 are injected (**$p < 0.01$ for Wt α5; ***$p < 0.001$ for α5 D397N). The D397N variant shows significantly stronger competition with β4 compared with Wt α5 (*$p < 0.05$). Triangles indicate increasing relative amounts of one specified subunit. ***B***, Representative traces of two-electrode voltage–clamp recordings. ***C***, Schematic representation of β2/β4 chimeras indicating the domains, motifs, or residues exchanged between β4 (green) and β2 (black) subunits and corresponding amino-acid number and substitutions (left). Fold current increase (right) indicates the relative current amplitude of nicotine-evoked currents for each β2/β4 chimera expressed with the α3 subunit at 1:10 relative to 1:1 ratio. All values are expressed as mean ± SEM; $n$ = 5 per ratio in all experiments.

NOTES

***Transgenic mice of the* Chrnb4/a3/a5 *gene cluster (Tabac mice)***

To test the hypothesis that β4 is rate-limiting for nAChR assembly and function *in vivo* and that overexpression of β4 can strongly influence nicotine-evoked currents and behavioral responses to nicotine, we characterized a bacterial artificial chromosome (BAC) transgenic line spanning the *Chrnb4–Chrna3–Chrna5* gene cluster (Gong et al., 2003). The BAC transgene included the intact coding sequences of the *Chrnb4* gene, modified sequences of *Chrna3*, and incomplete sequences of *Chrna5*. *Chrna3* was modified by insertion of an enhanced green fluorescent protein (eGFP) cassette, followed by polyadenylation signals at the ATG translation initiator codon of *Chrna3* (Fig. 2A). The upstream sequences of *Chrna5*, encoding exon 1 splice variants (Flora et al., 2000), are missing in the BAC transgene (Fig. 2A). To promote correct expression of *Chrnb4*, the BAC included the intergenic and 5' flanking regions encompassing the *cis*-regulatory elements that coordinate cotranscriptional control of the genes in the cluster (Bigger et al., 1997; Xu et al., 2006; Medel and Gardner, 2007).

As a result of these modifications in the BAC transgene, these mice (referred to as Tabac mice for Transgenic a3b4a5 cluster) express high levels of β4

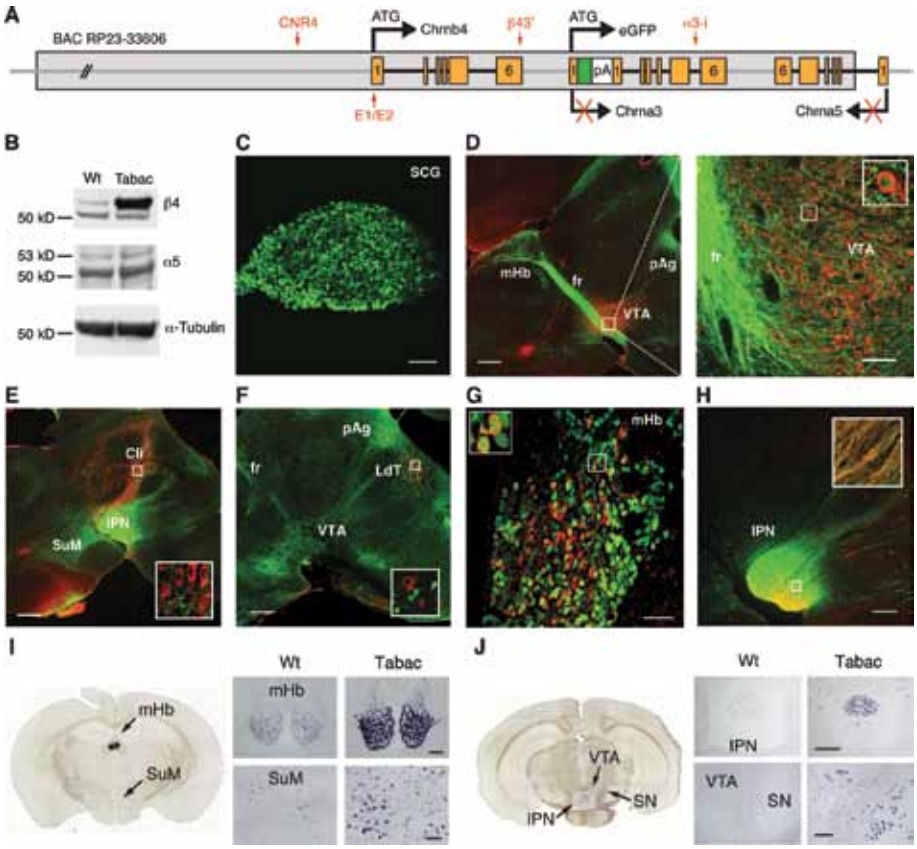


Figure 2. Tabac mice express elevated *Chrnb4* transcripts in *Chrna3*-eGFP labeled neurons. ***A***, Scheme of the modified mouse BAC containing the *Chrnb4–Chrna3–Chrna5* gene cluster. Yellow boxes, exons; green box, eGFP cassette; white box, polyadenylation signal (pA); black arrows, direction of transcription; red crosses, truncated transcription; *cis*-regulatory elements marked in red; CNR4, conserved noncoding region; β43' enhancer (Xu et al., 2006); E1/E2, SP1, and SP3 binding sites (Bigger et al., 1997); α3-i, transcriptional silencer (Medel and Gardner, 2007). ***B***, Western blot analyses of β4 (53 kD), α5 (2 splice variants: 50 kD and 53 kD), and α-Tubulin in brain extracts of Wt and Tabac mice. ***C–H***, eGFP-expressing neurons (green) in peripheral SCG (***C***) and in sagittal brain sections (except ***G***, coronal) of Tabac mice immunostained with TH (***D*** and ***E***) and ChAT (***F–H***) in red. ***I***, ***J***, *In situ* hybridization of *Chrnb4* transcripts in Wt and Tabac brain sections. fr, fasciculus retroflexus; LdT, laterodorsal tegmentum; pAg, periaqueductal gray; SCG, superior cervical ganglia; SN, substantia nigra. Scale bars: ***C***, 100 μm; ***D–F,*** 500 μm (magnification of ***D*** is indicated by the dotted lines; scale bar, 50 μm); ***G***, 50 μm; ***H***, 250 μm; mHb, 100 μm; SuM, 50 μm; IPN, 250 μm; VTA, 100 μm.

but not α5 (Fig 2*B*), and expression of α3 is replaced by expression of an eGFP reporter cassette to monitor the sites expressing the transgene (Fig. 2*C–H*). As shown in Figure 2, neurons expressing eGFP were evident in autonomic ganglia (Fig. 2*C*) and in very restricted brain structures (Figs. 2*D–H*) known to express these genes (Zoli et al., 1995). Immunostaining with cholinergic (choline acetyltransferase [ChAT]) and dopaminergic (tyrosine hydroxylase [TH]) markers indicated high expression of *Chrna3*/eGFP in cholinergic neurons of the Hb–IPN system (Fig. 2*G,H*). Intense *Chrna3*/eGFP expression was also detected in other brain areas (Fig. 3*D,E*) involved in nicotine addiction, such as the ventral tegmental area (VTA), the caudal linear nucleus (Cli), the supramammilary nucleus (SuM) (Ikemoto et al., 2006), and the laterodorsal tegmental nucleus (Fig. 2*F*), which provides modulatory input to the VTA (Maskos, 2008).

We performed *in situ* hybridization experiments to verify that the BAC accurately directed expression of transgenic *Chrnb4* transcripts to eGFP-positive brain areas. Tabac mice showed a prominent enrichment of *Chrnb4* transcripts in α3β4*-positive areas such as the mHb and IPN, and in brain areas that have been shown to express lower levels of *Chrnb4*, such as SuM (Dineley-Miller and Patrick, 1992) and VTA (Yang et al., 2009) (Fig. 2*I,J*). Reverse transcriptase (RT)–PCR studies showed that *Chrna4*, *Chrna7*, and *Chrnb2* transcripts (which are not present in the BAC) are not altered in Tabac mice (data not shown). Taken together, these data show that Tabac mice express high levels of β4, but not α5, in α3/eGFP–labeled cells in CNS and PNS structures known to express the *Chrnb4–Chrna3–Chrna5* nicotinic gene cluster. Thus, they provide a useful mouse model to test the consequences of enhanced β4 expression at endogenous sites.

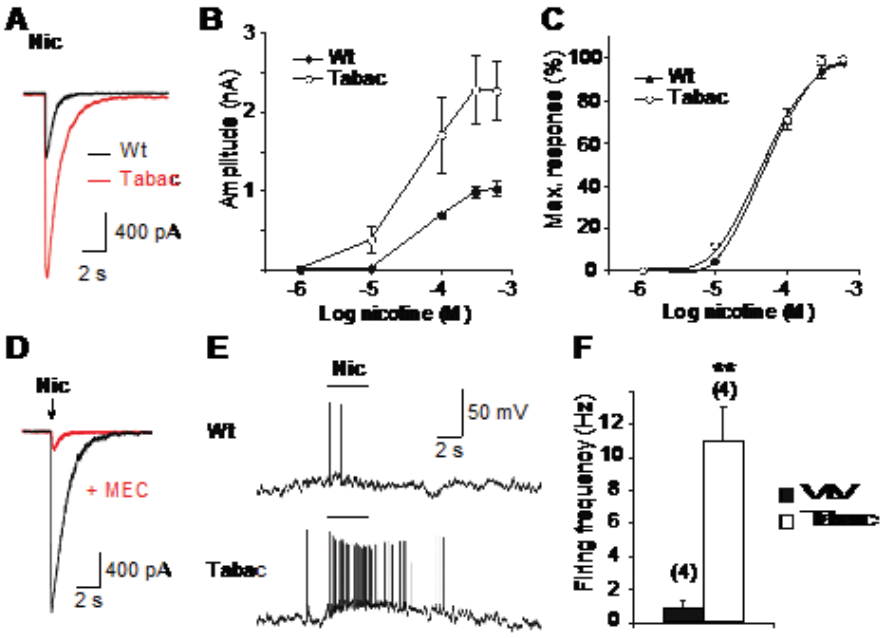


**Figure 3.** Tabac mice show increased α3β4* nAChR nicotine-evoked currents and firing frequency in *Chrna3*-eGFP–labeled neurons. ***A–F***, Whole-cell patch–clamp recordings of mHb neurons in acute brain slices from Wt and Tabac mice. Representative traces of nicotine-evoked currents (***A***, 100 μM, 50 ms application) and corresponding concentration-response relationships (***B***, peak amplitudes ± SEM; $n = 5–8$ cells per genotype; $p < 0.05$ by 2-way ANOVA). Dose-response curves in ***C*** were calculated relative to the maximal response to nicotine from ***B***. ***D***, Mecamylamine (MEC) (3 μM, 3 min) inhibition of nicotine-evoked currents in neurons of Tabac mice. Representative current–clamp recordings (***E***) and quantification of action potentials upon local application of nicotine (1 μM, 3 s) in neurons of Wt and Tabac mice (***F***, mean firing frequency ± SEM; $n = 4$; $p < 0.01$). Numbers in parentheses represent number of neurons tested. All values expressed as mean ± SEM.

NOTES

***Increased nicotine-evoked currents in transgenic Tabac mice***

Given the demonstration that the level of β4 expression is rate-limiting for the function of α3β4α5 receptors *in vitro* (Fig. 1), we were next interested in determining whether enhanced expression of *Chrnb4* in Tabac neurons resulted in elevated nicotine-evoked currents *in vivo*. Previous studies have shown that neurons in the mHb express high levels of α3β4α5 receptors (Quick et al., 1999). Accordingly, we employed patch–clamp recordings to measure nicotine-evoked currents in mHb neurons of Tabac mice. A large proportion of mHb neurons in Wt mice ($n = 20$ of $N = 23$ neurons recorded) responded to local fast application (50 ms) of nicotine (Fig. 4*A*,*B*). In *Chrna3*/eGFP–labeled mHb neurons of Tabac mice, nicotine elicited significantly increased peak currents in comparison with Wt littermates (on average, 3.4-fold at 100 μM nicotine, two-way ANOVA $p < 0.05$) (Fig. 3*B*). Similarly increased responses were obtained using acetylcholine (ACh) (data not shown). Dose-response curves for nicotine showed no significant differences between Wt and Tabac mice, indicating that the affinity of the receptors in the transgenic mice is not altered (Fig 3C). Application of mecamylamine, a nonselective potent inhibitor of α4β2* and α3β4* nAChRs (Bacher et al., 2009), resulted in a blockade of as much as 90% of the nicotine-elicited responses in Tabac mice (Fig. 3*D*). This finding demonstrates that the enhanced nicotine responses in Tabac neurons result directly from elevated levels of functional nAChRs.

To determine whether these additional receptors cause enhanced neuronal excitability, the firing rate of habenular neurons was measured in current–clamp assays in response to nicotine. Neurons from Wt and Tabac mice were silent at rest (–70 mV). Local nicotine application (1 μM for 3 s) elicited single action potentials in Wt neurons, whereas nicotine induced a robust burst of action potentials with a 13-fold higher firing frequency on average in Tabac neurons ($p < 0.005$) (Fig. 4*E*,*F*). Together, these results indicate that the increased sensitivity of mHb neurons to nicotine in Tabac mice results from the presence of additional functional nAChRs rather than from changes in the nicotine affinity of existing receptors.

## Tabac mice show strong aversion to nicotine consumption, and display nicotine-conditioned place aversion

We were next interested in the effects of elevated nAChR expression on the behavioral responses of Tabac mice to nicotine. Measurements of drinking volumes showed that Tabac mice consumed significantly less nicotine-containing water than Wt littermates (Fig. 4*A*,*B*). Because nicotine solutions have a bitter taste, nicotine was diluted in saccharin solution, and control experiments with a bitter solution (containing quinine) were performed. There were no differences in consumption of regular, sweetened, or bitter water between the two groups (Fig. 4*A*).

Next, we performed a free-choice consumption experiment in which mice were allowed to choose between regular water and water supplemented with different concentrations of nicotine (1–100 μg/ml) without saccharin. Analysis of the nicotine volume consumed relative to the total fluid intake (Fig. 4C) indicated that Tabac mice significantly avoided drinking nicotine solutions containing more than 5 μg/ml nicotine ($p < 0.05$; two-way ANOVA), while Wt showed no preference between water and nicotine solutions below 50 μg/ml and avoided drinking the highest concentration of nicotine solution tested. It is possible that the decrease in drinking resulted from the negative consequences of hyperactivation of the autonomic nervous system, leading to gastric distress or nausea. However, we observed no significant differences in body weight (Fig. 4*D*), micturition, and digestion before and during the nicotine consumption experiments.

As an independent measure of the effects of nicotine in Tabac mice, conditioned place aversion (CPA) assays were performed. Because conditioning to nicotine is dependent on both concentration and strain (O'Dell and Khroyan, 2009), we measured CPA in Wt C57BL/6 littermates at 0.5 mg nicotine/kg body weight. Under these conditions, we observed neither a preference for nor an aversion to nicotine. In contrast, strong conditioned place aversion to nicotine was observed in Tabac mice (Fig. 4*E*). These data both confirm the conclusions of the nicotine consumption assays and demonstrate that negative reward learning associated to nicotine is strongly increased in Tabac mice. We conclude that overexpression of the β4 subunit *in vivo* leads to an increase in functional α3β4* receptors, resulting in a higher sensitivity to the aversive properties of nicotine.

## Lentiviral-mediated expression of the α5 D397N variant in the medial habenula reverses nicotine aversion in Tabac mice

Our observations showed that the α5 D397N variant reduces α3β4α5 nicotine-evoked currents in oocytes (Fig. 1) and that the mHb contains a high density of native α5 nAChR subunits in combination with α3β4 subunits (Fig. 2). They suggested that the enhanced nicotine aversion evident in Tabac mice could be

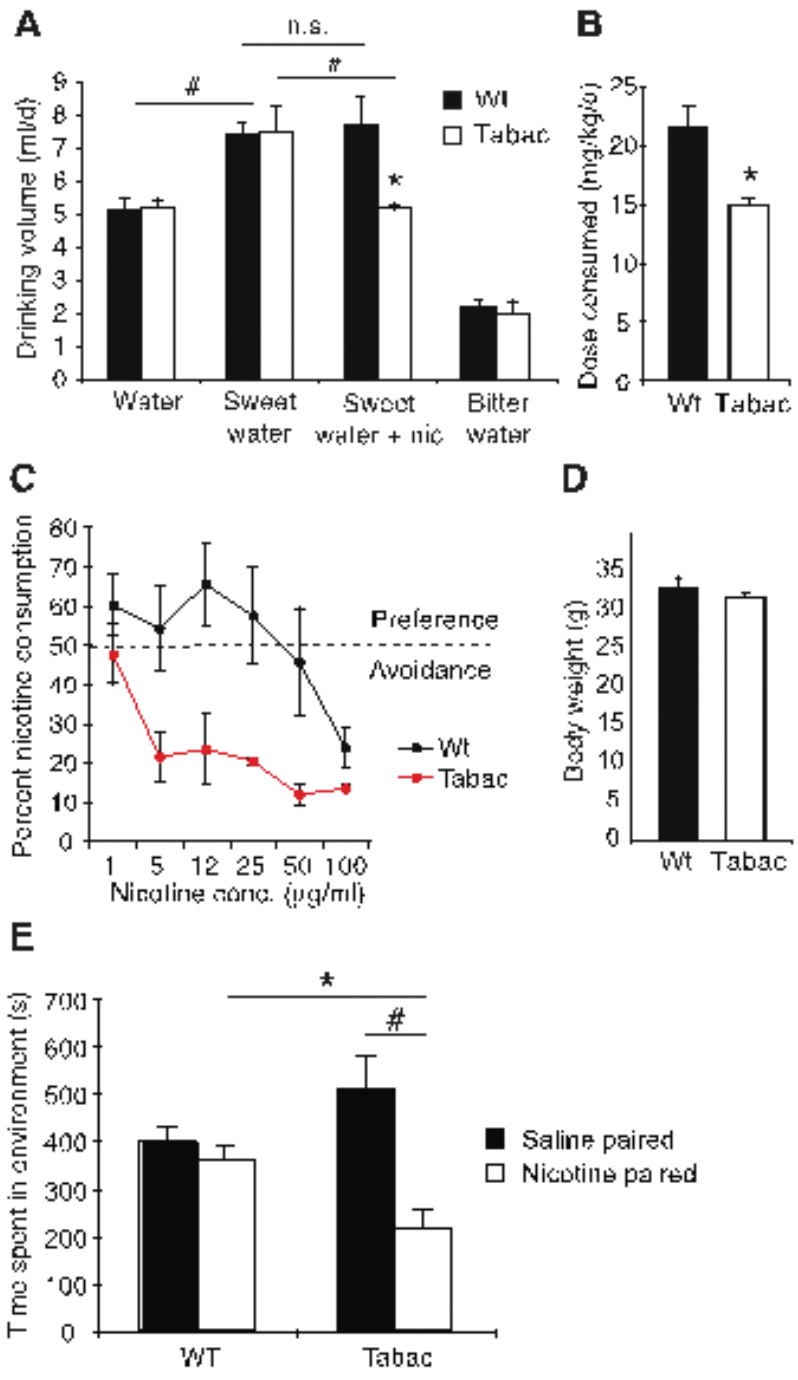


Figure 4. Tabac mice consume less nicotine and show conditioned place aversion. ***A***, ***B***, Nicotine consumption in a no-choice paradigm (1 drinking bottle). ***A***, Drinking volumes (ml/mouse/day) of water, sweet water (2% saccharine), and bitter water (5 mM quinine). The tested period of consumption was 3 d (paired t test; $p < 0.05$). ***B***, The dose of nicotine consumed expressed as the mg of nicotine consumed per day considering the body weight of the mouse (mg/kg/d) ($p < 0.05$). Wt mice ($n = 10$); Tabac mice ($n = 10$). ***C***, Nicotine consumption in a two-bottle-choice paradigm between water and water containing the indicated nicotine concentrations, expressed as percent of the volume of nicotine solution consumed divided by the total fluid intake and per day. Each concentration was tested for 3 d. Dashed line at 50% indicates no preference. Wt mice ($n = 7$); Tabac mice ($n = 6$); two-way ANOVA; $p < 0.05$. ***D***, Body weight of Wt and Tabac mice after nicotine drinking tests. ***E***, Nicotine administration (0.5 mg/kg) elicits place aversion to nicotine-paired environment in Tabac mice. Following conditioning, Tabac mice preferred the saline-paired environment over the nicotine-paired environment (paired *t* test; $p < 0.05$). Wt mice spent significantly more time in the nicotine-paired environment compared with Tabac mice (*$p < 0.05$). Wt mice ($n = 7$); Tabac mice ($n = 6$). Data are expressed as time spent in drug-paired environments after drug conditioning. All values are expressed as mean ± SEM.

NOTES

reversed by expression of the α5 variant in the mHb. To test this hypothesis, we employed lentiviral vector–mediated transduction to express the α5 D397N in mHb neurons of Tabac mice. We bilaterally injected either control lentivirus (LV-PC) or the LV-α5 D397N (LV-α5N) viruses in Tabac mice. As shown in Figure 5*B*, immunostaining for the mCHERRY reporter of LV-α5N expression or direct fluorescence derived from the control LV demonstrated that the lentiviral-transduced area corresponds with that occupied by α3β4*-eGFP–labeled neurons in the mHb of Tabac mice.

Given that the maximal difference in nicotine consumption in Tabac mice occurred at 25 μg/ml nicotine (Fig. 5C), mice were again given a two-bottle choice test to measure nicotine aversion. These experiments were performed in Tabac mice backcrossed to the inbred mouse line C57/BL6 (Fig. 5C), which has been shown to have a high basal level of self-selection of nicotine (Meliska et al., 1995; Robinson et al., 1996; Glatt et al., 2009), and in Tabac mice outbred between FBV/N mixed and Swiss Webster (Fig. 5*D*). As shown in Figure 5C, in C57/BL6 Tabac mice, injection of the LV-α5N virus reversed their nicotine aversion compared with mice injected with the control virus. In outbred Tabac mice, we observed no alteration in nicotine aversion in Tabac mice injected with the control virus (Fig. 5*D*) with respect to uninjected Tabac mice (Fig. 5C). Importantly, infection with LV-α5N virus reversed nicotine aversion in Tabac mice (Fig. 5*D*), restoring nicotine consumption in α5D397N-

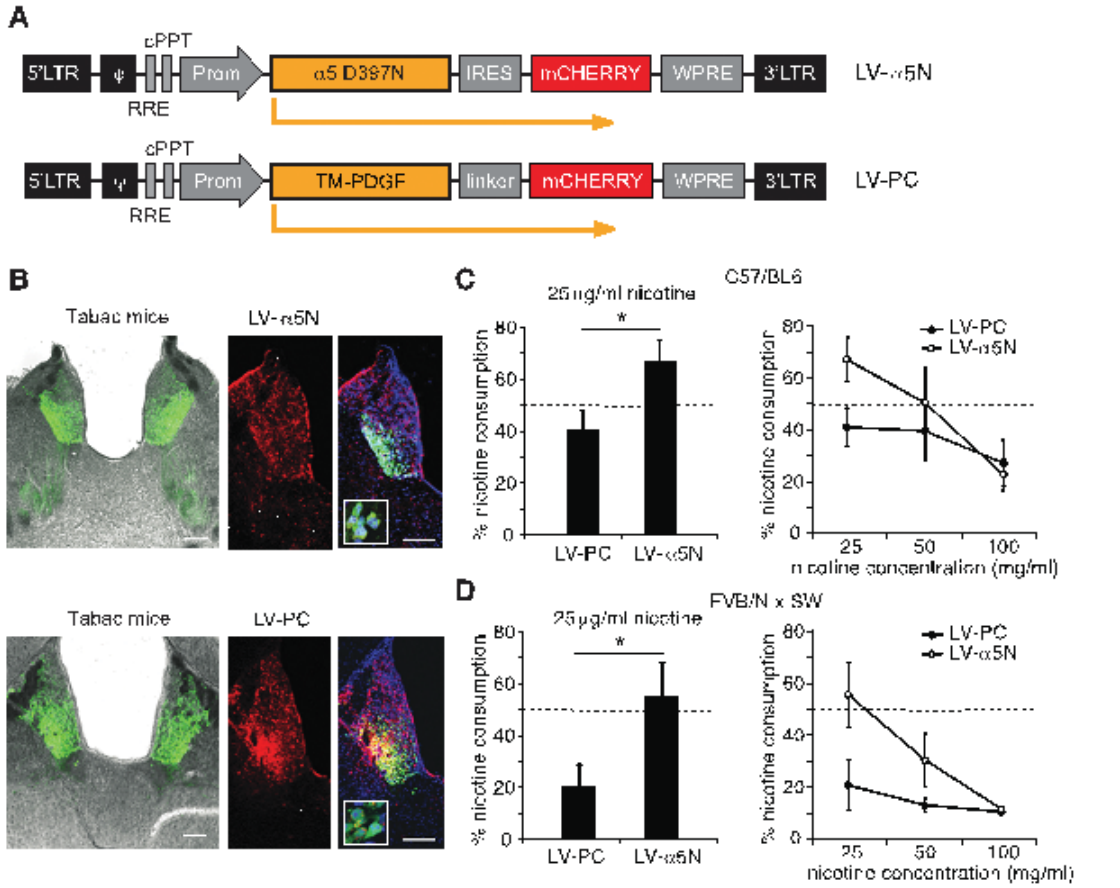


**Figure 5.** Reversal of nicotine aversion in Tabac mice by lentiviral vector–mediated expression of the α5 D397N variant in the mHb. ***A***, Schematic representation of the lentiviral (LV) constructs used for brain stereotactic injections. LV-α5N carries the mouse α5 variant D397N followed by an IRES and the mCHERRY reporter. The control virus (LV-PC) carries mCHERRY fused to the N-terminus of the transmembrane domain of the platelet-derived growth factor receptor (TM-PDGF) via a linker domain. ***B***, Coronal brain sections of Tabac mice stereotactically injected in the mHb with the indicated lentivirus. Colocalization of eGFP fluorescence driven by the transgene in Tabac mice and mCHERRY red fluorescence for LV-PC, or mCHERRY immunofluorescence for mice injected with LV-α5N. Two-bottle choice nicotine consumption in Tabac mice after stereotactic bilateral injection of control (LV-PC) and mutated α5 (LV-α5N) lentiviral constructs in the mHb. Tabac mice backcrossed to C57BL6; $n = 4$ for LV-PC; $n = 5$ for LV-α5N; $p < 0.05$ (C) and Tabac mice hybrid of FVB/N and Swiss Webster; $n = 8$ for LV-PC; $n = 9$ for LV-α5N (D). IRES, internal ribosomal entry site; LTR, long terminal repeat; WPRE, woodchuck postregulatory element. Scale bars: ***B, C, D***, 100 μm.

infected Tabac mice to levels evident in Wt mice (Fig. 5C). These results demonstrate a major role for the mHb in nicotine consumption.

## Discussion

Human genetic studies have established an association between the *Chrnb4–CHRNA3–CHRNA5* locus and tobacco use (Thorgeirsson et al., 2008; Weiss et al., 2008; Saccone et al., 2009; Amos et al., 2010b). Here we report a novel mouse model (Tabac mice) with altered nicotine consumption and conditioned place aversion caused by elevated levels of β4, enhanced nicotine-evoked currents, and increased surface expression of functional nAChRs at endogenous sites. The ability of β4 to enhance nicotine-evoked currents depends on a single critical residue (S435) located in the intracellular vestibule of the receptor. Interestingly, modeling studies revealed that one of the most common SNPs associated with tobacco usage, D398N in the α5 subunit, also maps to this domain. Functional analyses of this variant demonstrate that alterations in this domain can result in profound effects on nicotine-evoked currents. Based on our studies in Tabac mice in which enhanced current is associated with increased aversion to nicotine, we predicted that the α5 variant (corresponding to D397N in mice) should increase nicotine consumption consistent with its association with smoking. To test this idea, and given that the mHb contains a very high concentration of endogenous α3β4α5 receptors, as well as elevated levels of β4 driven by the Tabac transgene, we introduced the α5 variant by viral-mediated transduction in habenular neurons of Tabac mice. The reversal of the nicotine aversion achieved in Tabac mice observed in these experiments demonstrates that the mHb plays a major regulatory role in nicotine consumption.

Three main points are addressed in this study. First, changes both in the coordinated expression of α3β4α5 subunits (i.e., overexpression of the β4 subunit) as well as in single residues (i.e., *in vivo* viral-mediated expression of the α5 D397N variant) have a strong influence on nicotine consumption in mice. This is consistent with recent genome-wide association studies that have identified SNPs in both regulatory and coding regions of the *Chrnb4–CHRNA3–CHRNA5* gene cluster that are associated with nicotine dependence (Levitin et al., 2008; Thorgeirsson et al., 2008; Saccone et al., 2009). Thus, our studies provide a new model for further exploration of the involvement of α3β4α5 nAChR function in nicotine consumption.

Second, our studies demonstrate that the intracellular vestibule of the α3β4α5 receptor exerts an important effect on nicotine-evoked currents. The high concentration of charges in this membrane-associated domain is conserved in the superfamily of Cys-loop receptors (Kelley et al., 2003; Unwin, 2005; Carland et al., 2009). Electrostatic calculations by homology with the *Torpedo* nAChR predict that α3β4α5 receptors form a highly electronegative vestibule most likely to promote a stabilizing environment for cation outflow. The change in current amplitude produced by substitutions of charged residues (S435R and D397N) in this domain of the receptor predicts that alterations of the electrostatic charge of the vestibule are critical for receptor function. This finding is consistent with studies of the inner vestibule in other Cys-loop receptor channels. For example, in 5HT3A receptors, the substitution of arginine-positive residues increased channel conductance, whereas introduction of basic residues in this domain of α1 glycine receptors decreases glycine-evoked currents (Kelley et al., 2003; Carland et al., 2009). Numerous reports have linked the α5 D398N polymorphism to smoking incidence (Saccone et al., 2009; Bierut, 2008, 2010). Incorporation of D398N α5 variant into α4β2-containing receptors in transfected cells results in a twofold reduction in epibatidine-evoked calcium currents without a change in surface expression (Bierut et al., 2008), consistent with the reduction in nicotine-evoked current amplitudes reported here upon incorporation of this variant into α3β4 containing nAChRs.

Taken together, these observations support the hypothesis that substitution of this charged residue modifies the vestibule electrostatic charge but not the number of receptors incorporated into the plasma membrane. In contrast, the increase in receptor-surface expression in Tabac mice and the identification of a single unique residue in the β4 subunit (S435R) suggest that the β4 subunit is rate-limiting for the formation of α3β4α5 nAChRs. S435R is essential for the increase of currents observed in this study upon overexpression of the β4 subunit; further, S435R can confer this property to β2 subunits. Although the precise role of S435 is not yet clear, it may be involved in stabilizing nAChR complexes, export of the receptors from the endoplasmic reticulum, interactions with trafficking proteins, or alterations in its turnover from the cell surface. For example, rapsyn binding to the α-helical domains corresponding to the inner vestibule of α1β1γδ nAChR is required for surface expression of this receptor (Lee et al., 2009). It also has been shown that binding of UBXD4 to the cytoplasmic loop of α3 can interfere with its ubiquitination and, consequently, the number of α3-containing receptors at the cell surface (Rezvani et al., 2010). Thus,

NOTES

NOTES

our studies point to two mechanisms mediated by specific residues in the inner vestibule: one leading to ion permeation changes within a single α3β4α5 receptor and the other leading to increased surface expression of receptors by native β4.

Third, the studies presented here demonstrate that the mHb has a major influence on the control of nicotine consumption. These studies extend the findings from previous studies on the role of the habenula in nicotine withdrawal and drug addiction (Taraschenko et al., 2007; Jackson et al., 2008; Salas et al., 2004, 2009) and, recently, in nicotine self-administration (Fowler et al., 2011). Although multiple interconnected brain regions, including the prefrontal cortex, VTA, thalamus, striatum, and amygdala, are affected by chronic use of nicotine, the habenular system is emerging as an important station in pathways regulating the behavioral effects of nicotine (Rose, 2007; De Biasi and Salas, 2008; Changeux, 2010). The mHb projects mainly to the IPN, which, in turn, seems to inhibit the motivational response to nicotine intake. Thus, inactivation of the mHb and IPN both result in increased intake of nicotine (Fowler et al., 2011). Consistent with these studies, overexpression of β4 results in enhanced activity of the mHb, resulting in the opposing effect: aversion to nicotine. Reversal of nicotine aversion in Tabac mice overexpressing β4 is achieved by expression of the α5 D397N in mHb neurons. Similarly, α5 re-expression in the habenula of α5 KO mice normalizes their nicotine intake (Fowler et al., 2011).

Taken together, these studies provide direct evidence that the mHb acts as a gatekeeper in the control of nicotine consumption and that the balanced contribution of β4 and α5 subunits is critical for this function. Further analyses of nAChR function in the habenulo-IPN tract and its associated circuitry will be required to fully understand the addictive properties of nicotine.

## References


Amos CI, Gorlov IP, Dong Q, Wu X, Zhang H, Lu EY, Scheet P, Greisinger AJ, Mills GB, Spitz MR (2010a) Nicotinic acetylcholine receptor region on chromosome 15q25 and lung cancer risk among African Americans: a case-control study. J Natl Cancer Inst 102:1199-1205.

Amos CI, Spitz MR, Cinciripini P (2010b) Chipping away at the genetics of smoking behavior. Nat Genet 42:366-368.

Bacher I, Wu B, Shytle DR, George TP (2009) Mecamylamine—a nicotinic acetylcholine receptor antagonist with potential for the treatment of neuropsychiatric disorders. Expert Opin Pharmacother 10:2709-2721.

Bierut LJ (2010) Convergence of genetic findings for nicotine dependence and smoking related diseases with chromosome 15q24-25. Trends Pharmacol Sci 31 46-51.

Bierut LJ, Stitzel JA, Wang JC, Hinrichs AL, Grucza RA, Xuei X, Saccone NL, Saccone SF, Bertelsen S, Fox L, Horton WJ, Breslau N, Budde J, Cloninger CR, Dick DM, Foroud T, Hatsukami D, Hesselbrock V, Johnson EO, Kramer J, et al. (2008) Variants in nicotinic receptors and risk for nicotine dependence. Am J Psychiatry 165:1163-1171.

Bigger CB, Melnikova IN, Gardner PD (1997) Sp1 and Sp3 regulate expression of the neuronal nicotinic acetylcholine receptor beta4 subunit gene. J Biol Chem 272:25976-25982.

Carland JE, Cooper MA, Sugiharto S, Jeong HJ, Lewis TM, Barry PH, Peters JA, Lambert JJ, Moorhouse AJ (2009) Characterization of the effects of charged residues in the intracellular loop on ion permeation in α1 glycine receptor channels. J Biol Chem 284:2023-2030.

Changeux JP (2010) Nicotine addiction and nicotinic receptors: lessons from genetically modified mice. Nat Rev Neurosci 11:389-401.

Dani JA, Heinemann S (1996) Molecular and cellular aspects of nicotine abuse. Neuron 16:905-908.

De Biasi M, Salas R (2008) Influence of neuronal nicotinic receptors over nicotine addiction and withdrawal. Exp Biol Med (Maywood) 233:917-929.

Dineley-Miller K, Patrick J (1992) Gene transcripts for the nicotinic acetylcholine receptor subunit, beta4, are distributed in multiple areas of the rat central nervous system. Brain Res Mol Brain Res 16:339-344.

Flora A, Schulz R, Benfante R, Battaglioli E, Terzano S, Clementi F, Fornasari D (2000) Transcriptional regulation of the human α5 nicotinic receptor subunit gene in neuronal and non-neuronal tissues. Eur J Pharmacol 393:85-95.

Fowler CD, Lu Q, Johnson PM, Marks MJ, Kenny PJ (2011) Habenular α5 nicotinic receptor subunit signalling controls nicotine intake. Nature 471:597-601.

Gahring LC, Rogers SW (2010) Nicotinic receptor subunit α5 modifies assembly, up-regulation, and response to pro-inflammatory cytokines. J Biol Chem 28526049-26057.

NOTES

Glatt AR, Denton K, Boughter JD Jr (2009) Variation in nicotine consumption in inbred mice is not linked to orosensory ability. Chem Senses 34:27-35.

Gong S, Zheng C, Doughty ML, Losos K, Didkovsky N, Schambra UB, Nowak NJ, Joyner A, Leblanc G, Hatten ME, Heintz N (2003) A gene expression atlas of the central nervous system based on bacterial artificial chromosomes. Nature 425:917-925.

Gotti C, Clementi F, Fornari A, Gaimarri A, Guiducci S, Manfredi I, Moretti M, Pedrazzi P, Pucci L, Zoli M (2009) Structural and functional diversity of native brain neuronal nicotinic receptors. Biochem Pharmacol 78:703-711.

Ikemoto S, Qin M, Liu ZH (2006) Primary reinforcing effects of nicotine are triggered from multiple regions both inside and outside the ventral tegmental area. J Neurosci 26:723-730.

Jackson KJ, Martin BR, Changeux JP, Damaj MI (2008) Differential role of nicotinic acetylcholine receptor subunits in physical and affective nicotine withdrawal signs. J Pharmacol Exp Ther 325:302-312.

Kedmi M, Beaudet AL, Orr-Urtreger A (2004) Mice lacking neuronal nicotinic acetylcholine receptor beta4-subunit and mice lacking both α5- and β4-subunits are highly resistant to nicotine-induced seizures. Physiol Genomics 17:221-229.

Kelley SP, Dunlop JI, Kirkness EF, Lambert JJ, Peters JA (2003) A cytoplasmic region determines single-channel conductance in 5-$HT_3$ receptors. Nature 424:321-324.

Lee Y, Rudell J, Ferns M (2009) Rapsyn interacts with the muscle acetylcholine receptor via alpha-helical domains in the alpha, beta, and epsilon subunit intracellular loops. Neuroscience 163:222-232.

Levitin F, Weiss M, Hahn Y, Stern O, Papke RL, Matusik R, Nandana SR, Ziv R, Pichinuk E, Salame S, Bera T, Vincent J, Lee B, Pastan I, Wreschner DH (2008) *PATE* gene clusters code for multiple, secreted TFP/Ly-6/uPAR proteins that are expressed in reproductive and neuron-rich tissues and possess neuromodulatory activity. J Biol Chem 283:16928-16939.

Lu B, Su Y, Das S, Wang H, Wang Y, Liu J, Ren D (2009) Peptide neurotransmitters activate a cation channel complex of NALCN and UNC-80. Nature 457:741-744.

Maskos U (2008) The cholinergic mesopontine tegmentum is a relatively neglected nicotinic master modulator of the dopaminergic system: relevance to drugs of abuse and pathology. Br J Pharmacol 153(Suppl 1):S438-S445.

Maskos U, Molles BE, Pons S, Besson M, Guiard BP, Guilloux JP, Evrard A, Cazala P, Cormier A, Mameli-Engvall M, Dufour N, Cloëz-Tayarani I, Bemelmans AP, Mallet J, Gardier AM, David V, Faure P, Granon S, Changeux JP (2005) Nicotine reinforcement and cognition restored by targeted expression of nicotinic receptors. Nature 436:103-107.

McGehee DS, Role LW (1995) Physiological diversity of nicotinic acetylcholine receptors expressed by vertebrate neurons. Annu Rev Physiol 57:521-546.

Medel YF, Gardner PD (2007) Transcriptional repression by a conserved intronic sequence in the nicotinic receptor α3 subunit gene. J Biol Chem 282:19062-19070.

Meliska CJ, Bartke A, McGlacken G, Jensen RA (1995) Ethanol, nicotine, amphetamine, and aspartame consumption and preferences in C57BL/6 and DBA/2 mice. Pharmacol Biochem Behav 50:619-626.

Nashmi R, Dickinson ME, McKinney S, Jareb M, Labarca C, Fraser SE, Lester HA (2003) Assembly of α4β2 nicotinic acetylcholine receptors assessed with functional fluorescently labeled subunits: effects of localization, trafficking, and nicotine-induced upregulation in clonal mammalian cells and in cultured midbrain neurons. J Neurosci 23:11554-11567.

O'Dell LE, Khroyan TV (2009) Rodent models of nicotine reward: what do they tell us about tobacco abuse in humans? Pharmacol Biochem Behav 91:481-488.

Picciotto MR (1998) Common aspects of the action of nicotine and other drugs of abuse. Drug Alcohol Depend 51:165-172.

Quick MW, Ceballos RM, Kasten M, McIntosh JM, Lester RA (1999) α3β4 subunit-containing nicotinic receptors dominate function in rat medial habenula neurons. Neuropharmacology 38:769-783.

Ren XQ, Cheng SB, Treuil MW, Mukherjee J, Rao J, Braunewell KH, Lindstrom JM, Anand R (2005) Structural determinants of α4β2 nicotinic acetylcholine receptor trafficking. J Neurosci 25:6676-6686.

NOTES

Rezvani K, Teng Y, De Biasi M (2010) The ubiquitin-proteasome system regulates the stability of neuronal nicotinic acetylcholine receptors. J Mol Neurosci 40:177-184.

Robinson SF, Marks MJ, Collins AC (1996) Inbred mouse strains vary in oral self-selection of nicotine. Psychopharmacology (Berl) 124:332-339.

Rose JE (2007) Multiple brain pathways and receptors underlying tobacco addiction. Biochem Pharmacol 74:1263-1270.

Saccone NL, Wang JC, Breslau N, Johnson EO, Hatsukami D, Saccone SF, Grucza RA, Sun L, Duan W, Budde J, Culverhouse RC, Fox L, Hinrichs AL, Steinbach JH, Wu M, Rice JP, Goate AM, Bierut LJ (2009) The *CHRNA5–CHRNA3–Chrnb4* nicotinic receptor subunit gene cluster affects risk for nicotine dependence in African-Americans and in European-Americans. Cancer Res 69:6848-6856.

Salas R, Pieri F, De Biasi M (2004) Decreased signs of nicotine withdrawal in mice null for the β4 nicotinic acetylcholine receptor subunit. J Neurosci 24:10035-10039.

Salas R, Sturm R, Boulter J, De Biasi M (2009) Nicotinic receptors in the habenulo-interpeduncular system are necessary for nicotine withdrawal in mice. J Neurosci 29:3014-3018.

Scofield MD, Tapper AR, Gardner PD (2010) A transcriptional regulatory element critical for *Chrnb4* promoter activity *in vivo*. Neuroscience 170:1056-1064.

Tapper AR, McKinney SL, Nashmi R, Schwarz J, Deshpande P, Labarca C, Whiteaker P, Marks MJ, Collins AC, Lester HA (2004) Nicotine activation of α4* receptors: sufficient for reward, tolerance, and sensitization. Science 306:1029-1032.

Taraschenko OD, Shulan JM, Maisonneuve IM, Glick SD (2007) 18-MC acts in the medial habenula and interpeduncular nucleus to attenuate dopamine sensitization to morphine in the nucleus accumbens. Synapse 61:547-560.

Thorgeirsson TE, Geller F, Sulem P, Rafnar T, Wiste A, Magnusson KP, Manolescu A, Thorleifsson G, Stefansson H, Ingason A, Stacey SN, Bergthorsson JT, Thorlacius S, Gudmundsson J, Jonsson T, Jakobsdottir M, Saemundsdottir J, Olafsdottir O, Gudmundsson LJ, Bjornsdottir G, et al. (2008) A variant associated with nicotine dependence, lung cancer and peripheral arterial disease. Nature 452:638-642.

Unwin N (2005) Refined structure of the nicotinic acetylcholine receptor at 4A resolution. J Mol Biol 346:967-989.

Weiss RB, Baker TB, Cannon DS, von Niederhausern A, Dunn DM, Matsunami N, Singh NA, Baird L, Coon H, McMahon WM, Piper ME, Fiore MC, Scholand MB, Connett JE, Kanner RE, Gahring LC, Rogers SW, Hoidal JR, Leppert MF (2008) A candidate gene approach identifies the *CHRNA5-A3-B4* region as a risk factor for age-dependent nicotine addiction. PLoS Genet 4:e1000125.

Whiting PJ, Lindstrom JM (1988) Characterization of bovine and human neuronal nicotinic acetylcholine receptors using monoclonal antibodies. J Neurosci 8:3395-3404.

Xu W, Gelber S, Orr-Urtreger A, Armstrong D, Lewis RA, Ou CN, Patrick J, Role L, De Biasi M, Beaudet AL (1999) Megacystis, mydriasis, and ion channel defect in mice lacking the α3 neuronal nicotinic acetylcholine receptor. Proc Natl Acad Sci USA 96:5746-5751.

Xu X, Scott MM, Deneris ES (2006) Shared long-range regulatory elements coordinate expression of a gene cluster encoding nicotinic receptor heteromeric subtypes. Mol Cell Biol 26:5636-5649.

Yang K, Hu J, Lucero L, Liu Q, Zheng C, Zhen X, Jin G, Lukas RJ, Wu J (2009) Distinctive nicotinic acetylcholine receptor functional phenotypes of rat ventral tegmental area dopaminergic neurons. J Physiol 587:345-361.

Zoli M, Le Novere N, Hill JA Jr, Changeux JP (1995) Developmental regulation of nicotinic ACh receptor subunit mRNAs in the rat central and peripheral nervous systems. J Neurosci 15:1912-1939.

# Cell Types, Circuits, and Computation

Rava Azeredo da Silveira, PhD[1] and Botond Roska, PhD, MD[2]

[1]Department of Physics and Department of Cognitive Studies
École Normale Supérieure
Paris, France

[2]Neural Circuit Laboratories
Friedrich Miescher Institute for Biomedical Research
Basel, Switzerland

NOTES

## Introduction

The mammalian brain is assembled from thousands of neuronal cell types, organized into distinct circuits that perform computations relevant to behavior. Sophisticated local circuits exist in all brain regions and act in concert in the behaving animal. In order to gain insights into the brain's mechanistic functions, it is crucial to uncover what these local circuits are computing and how computations are achieved. Furthermore, understanding the changes that occur in neuronal circuits that are involved in specific brain diseases may help design strategies for therapy.

One of the most intriguing questions about local neuronal circuits pertains to the relation between structure and function: How does the connectivity of a circuit, together with the individual properties of the cell types that take part in it, result in a given computation? In this chapter, we review recent developments that begin to answer this question. We will look at examples of mammalian retinal circuits in which structure and function can be approached by means of genetic tools as well as by imaging and physiological techniques.

## The Retina as a Model System

The first steps of visual processing take place in the retina, which also serves as a unique model system for studying the relationship between structure and function. The retina is a self-contained system; that is to say, if the retina is involved in a particular neuronal computation, then one can understand the mechanisms of this computation by studying retinal circuits alone. This self-sufficiency results from the fact that, unlike fish and birds, mammals have minimal feedback from higher brain centers, which

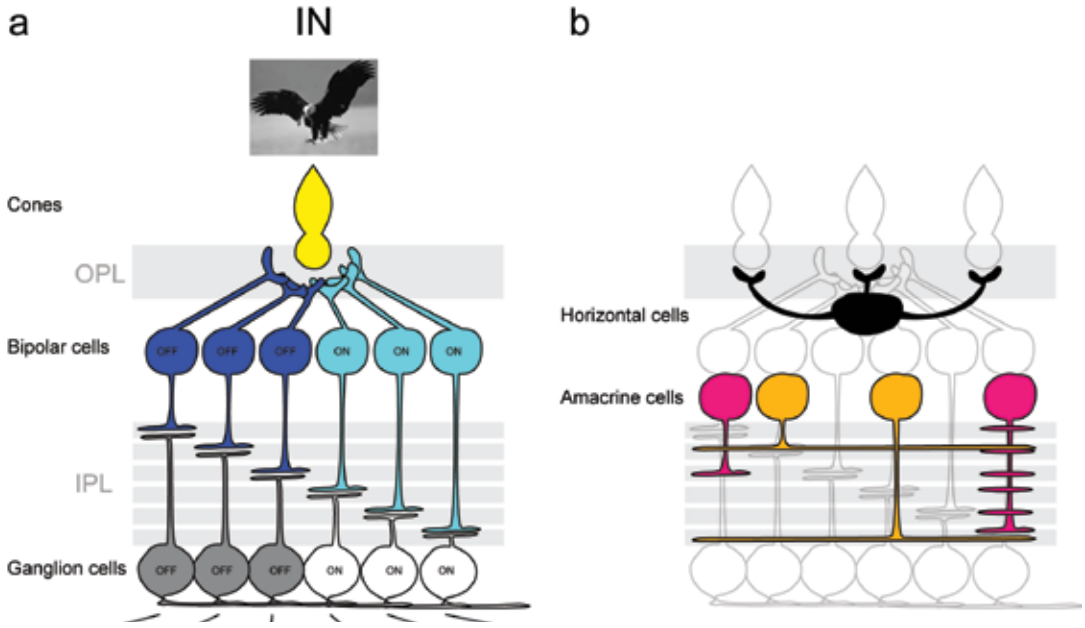


Figure 1. Functional organization of the mammalian retina. ***a***, The retina can be viewed as a parallel image processor that acquires movies (top panel) with its array of photoreceptors and uses its internal circuits to compute dozens of different neuronal representations (bottom panels) of the visual world. These are sent to higher brain centers via axons of the ganglion cells. Cone photoreceptors (middle panel, yellow), which are the light sensors in daylight, connect to ~10 types of bipolar cells. Half of the cone bipolar cells are activated by decrease (OFF cells, blue) and the other half by increase (ON cells, cyan) in light intensity. Axon terminals of OFF and ON bipolar cells settle at different depths within the inner plexiform layer (IPL): OFF terminals in the distal part and ON terminals proximally. Order exists at an even finer scale: bipolar cell terminals occupy one or a few of IPL strata (horizontal gray bars in the IPL). Dendrites of more than a dozen types of ganglion cells arborize in these strata and receive excitatory input from costratified bipolar cell terminals. The response polarity of a ganglion cell is determined by the types of bipolar cells that provide input to it: ON (white), OFF (gray), or ON–OFF. ***b***, The photoreceptor-to-bipolar synapse in the outer plexiform layer (OPL, top gray horizontal bar) is regulated by inhibitory horizontal cells (black). Similarly, excitatory synapses between bipolar and ganglion cells are modulated by inhibitory amacrine cells. These cells receive excitatory input from bipolar cells, and they provide feedback and feed-forward signals to bipolar terminals and ganglion cell dendrites, respectively. Amacrine cells are the most diverse of the retinal cells: >30 morphological types have been described. As yet, the functions of most of them are unknown. Amacrine cells are either GABAergic or glycinergic. GABA-releasing cells have long processes and are therefore called wide-field cells. Glycine-releasing cells have short processes, which often span several strata; these cells are often referred to as narrow-field cells. This architecture is further enriched by amacrine–amacrine cell inhibitory connections and by various electrical synapses within and among cell types.

NOTES

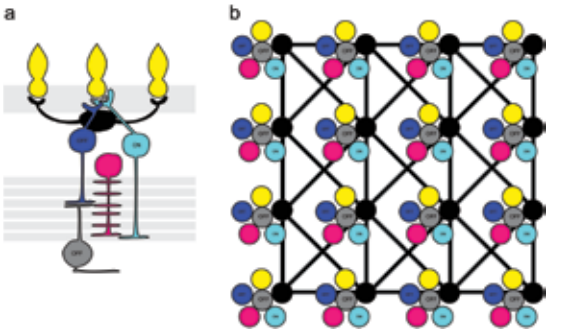


**Figure 2.** Retinal circuits are arranged in a mosaic. ***a***, Our current view of a retinal circuit: a few bipolar and a few amacrine cell types are involved in the circuit afferent to a ganglion cell. ***b***, These ganglion cell circuits are modular, since ganglion cells belonging to the same morphological and physiological type are arranged in a mosaic, each type with a different extent of dendritic overlap. (Color-coding of retinal cells as in Fig. 1)

possibly carry only modulatory commands. Thus, it is easy to isolate and maintain a healthy retina *in vitro*, and its natural inputs (dynamically evolving light patterns) can be presented to it in a controlled and quantitative manner. In probing the retina, neuronal activity from any cell class can be recorded.

In the past few decades, many investigations have pointed to the existence of specialized cell types and have found that these cell types are organized in local circuits. Cell types and circuits are ordered in neuronal layers in the retina (Fig. 1), which greatly simplifies the study of connectivity between neurons. The emerging picture is that each retinal output neuron—a ganglion cell—of a given type has an afferent circuit in which a few other cell types take part. Ganglion cell types are arranged in mosaics (Fig. 2) that display various degrees of overlap between the dendritic fields of the individual cells of the same type.

## The what and the how of retinal computation

Recent work from several groups suggests that the retina acts as the sum of many small devices—the circuits of different ganglion cell types—each highly stereotypical and task-specific. It appears that an appreciable fraction of these circuits is devoted to the analysis of different categories of motion. Eight types of direction-selective ganglion cells (four ON–OFF types, three ON types, and one OFF type) report either the direction of lateral object motion or the direction of global image drift. Approach motion is detected by at least one ganglion cell type, and other ganglion cell types respond to differential motion relative to global background motion. In all three cases of motion sensitivity — direction selectivity, approach sensitivity, and differential-motion sensitivity — the ganglion cells respond most vigorously to a so-called preferred stimulus, while their responses to so-called null stimuli are suppressed. In the case of the three motion categories, the preferred stimuli are lateral motion in a given direction, approach motion, and spatially differential motion, respectively; in contrast, null stimuli are lateral motion in the opposite direction, receding and lateral motion, and coherent whole-field motion, respectively. Yet another type of motion sensitivity consists in the suppression of response, in a few ganglion cell types, to the rapid image shifts that occur during wide-angle fast eye movements: the so-called saccades. Here the null stimulus (global image motion) is similar to that of the differential-motion sensitive cells, except that a high speed of global motion is required.

It is important to note that, in general, ganglion cells are broadly tuned: sensitivity does not mean exclusivity. Indeed, motion-sensitive cells do not respond only to their preferred stimulus. For example, an OFF direction-selective, approach-sensitive, or differential motion-sensitive cell will respond vigorously to a dark flash, as will any other OFF ganglion cell. The essence of motion sensitivity lies in the suppression of responses to null stimuli, that is, in what the motion-sensitive cell does not respond to.

When circuits afferent to motion-sensitive ganglion cells are examined in detail, the same two key elements of the computation emerge:

- First, the temporal or spatial modulation of response due to inhibition from amacrine cells;
- Second, nonlinearities both at bipolar cell terminals and in the way excitatory inputs from bipolar cells and inhibitory inputs from amacrine cells combine to produce spiking in the ganglion cell.

Other forms of nonlinearities are relevant to retinal computation. Owing to the spatiotemporal offset between excitation and inhibition and the manner in which the two inputs are summed, certain dynamical visual stimuli — the null stimuli — result in maximum inhibition and minimum excitation. Conversely, the preferred stimuli generate minimum inhibition and maximum excitation.

Intriguingly, but not surprisingly, the geometries of inhibitory cell types appear to be tailor-made for given computations. Starburst amacrine cells that provide inhibitory input to ON–OFF directional-selective ganglion cells are starlike, with long radial processes. The asymmetric inhibitory connectivity of these

NOTES

long processes to directional-selective ganglion cells, together with preferential release of neurotransmitters when the direction of motion points from the cell body to the tip of the processes, serve to produce directional selectivity. AII amacrine cells appear bushy and therefore span several retinal strata. This morphology allows these inhibitory cells to capture ON-bipolar inputs in daytime (cone-mediated) vision at the proximal strata, and to deliver them to approach-selective ganglion cells, which arborize in distal retinal strata. The dendritic trees of polyaxonal amacrine cells remain close to the cell body, while several axons radiate away from it. The cells require the ability to broadcast local input via long axons in all directions for inhibiting the response to global motion. The remarkable match between structure and function in these examples of retinal circuits suggests a long evolutionary process during which tinkering with details resulted in remarkably sophisticated computing devices.

The presence of diverse forms of nonlinearities is another factor that allows for the existence of task-specialized neuronal circuits. The active dendrites involved in direction selectivity provide what is perhaps the most striking example. In approach sensitivity and differential-motion sensitivity, nonlinear thresholding in bipolar or amacrine cells is key to making the respective computations. Nonlinear thresholding results in a nonlinear summation of inputs to the ganglion cell that originate from different subunits within its receptive field. As a result, the symmetry between ON and OFF stimuli, and hence between excitation and inhibition, may be broken. Furthermore, an array of nonlinear subunits feeding into a ganglion cell enables it to distinguish between (edge) motion and diffuse or wide-field temporal changes in light intensity.

## The relation between cell types, computation, and coding: open questions

Researchers have had much success in uncovering the categories of visual features that some ganglion cell types extract and isolating some elements of the neuronal circuits that give rise to the relevant computations. Nonetheless, we are still in an early phase of understanding the detailed structure of the retina and the array of mechanisms that rules its computational power. Three major sets of questions remain open.

### *Understanding the functional role of cell types in a given circuit*

First, at a physiological level, one would like to understand the functional role of all cell types involved in a given circuit. This program is ambitious, especially because of amacrine–amacrine interactions, which complicate the analysis. But the corollary, a simpler problem, is amenable to study: that of the functional role of cell types that synapse onto a ganglion cell type. The discovery of the detailed structure of hemoglobin paved the way toward revealing a great deal about the organization of amino acids into proteins. In much the same way, the elucidation of the computational role of the complete set of amacrine and bipolar cell types that belong to one identified ganglion cell type circuit may teach us basic principles about the roles of cell types in neuronal circuits.

### *Identifying preferred and null stimuli that correspond to each ganglion cell type*

Second, in order to understand vision at a more abstract, computational level, one would like to identify the preferred and null stimuli corresponding to each of the many ganglion cell types. But how can the wealth of the space of visual features be explored in a systematic and efficient way once a given ganglion cell type has been pinpointed? A number of methods have been devised to approach the problem of "feature selection" in the retina. These include linear–nonlinear models, covariance models, generalized linear models, and search procedures for maximally informative filters. Typically, these methods are designed to extract one or a few "features" — spatiotemporal light patterns — to which a ganglion cell or set of ganglion cells respond, out of a set of random stimuli. Experiments are now beginning to probe one cell type at a time and explore phenomenology that goes beyond mere feature selection. Thus, it is likely that theory, too, will require new machinery for extracting principles of computations. Currently, neither the choice of an appropriate set of stimuli nor the investigation of spatiotemporal nonlinearities is approached in either a systematic or a cogent manner.

### *Decoding the visual movie into precisely timed spikes in ganglion cells*

Third, the message that a ganglion cell type conveys to higher brain centers is coded in the spatiotemporal pattern of spikes produced by the entire mosaic of all ganglion cells of that particular type. What is the nature of the transformation that maps a visual movie into precisely timed spikes in all the members of a given cell type, and into correlations across cells of the same type? In order to begin answering this question, it will be desirable to develop methodologies that will allow the simultaneous recording of the spiking activity from a large fraction of the ganglion cells belonging to a genetically

NOTES

identified and morphologically confirmed mosaic of a given cell type.

## New technologies that relate structure to function

The emergence of new technologies points to the hope of approaching some of these questions in the near future. The specialized tasks that each of the many ganglion cell types are carrying out can be studied in detail, in a reasonable time frame, only if one can examine the same cell type whenever it is required. This technical challenge has hindered our understanding of ganglion cell computations for a long time, but in recent years, more than 100 mouse lines have been made and screened in which green fluorescent protein (GFP) is expressed in specific inner retinal (bipolar, amacrine, and ganglion cell) neuronal types or in combinations of a few types. Because GFP can be detected in live retinas, with the help of two-photon microscopy, one can now target many of the cell types for physiological recordings. In this context, the development of two-photon microscopy has been essential because its infrared laser does not bleach the photoreceptors and, therefore, light-evoked responses can be measured at different ambient intensities. These targeted recordings, together with visual stimulations, allow researchers to address the components (the what) of the circuit computation.

Once the visual features relevant to a ganglion cell type are identified, one would like to explain the corresponding computation based on the connectivity and the individual properties of the cell types that participate in the circuit. Technologies that enable efficient investigation of this "how" question are appearing on the horizon. Currently, two different approaches are being pursued: one relies on three-dimensional electron microscopy reconstructions, and the other uses transsynaptic viruses. Here we discuss the latter. The main requirement of the transsynaptic virus approach is having a transsynaptic tracer that passes from the postsynaptic cell to the presynaptic cells in a retrograde manner, and preferably monosynaptically. The difficulty lies in the initiation of the tracer from the ganglion cell type of interest. There are several ways of addressing this issue:

(1) In the rare scenario in which only one or a few ganglion cell types project to a specialized brain nucleus or initiate a reflex pathway, one can initiate the tracer from the target sites in vivo. The retinal circuits of melanopsin-containing and ON directional-selective cells, for example, were investigated in this way;

(2) If the ganglion cell type of interest expresses Cre recombinase, it is possible to conditionally initiate the tracer in vivo; and

(3) Jump-starting the tracer from a recorded single ganglion cell ex vivo and culturing the retina for a few days would allow for the visualization of the presynaptic cells after each recording.

Confirming functional connectivity between the virus-labeled cells requires dual patch–clamp experiments or, perhaps preferably, the development of tracers that express light-activated channels. Since, at present, the tracers are viruses that can be genetically engineered, equipping them with light-activated channels or pumps and/or Ca sensors would allow synaptic strengths to be determined and dendritic and axonal activity patterns to be imaged. Finally, the ligand-mediated silencing of the presynaptic cell type during the corresponding visual computation would be an important step in relating the activity of a presynaptic cell type to the visual features extracted by a ganglion cell efferent to it.

## The fate of "retinal movies"

The existence of a large number of parallel features extracted from visual scenes and projected by the retina to higher brain centers poses an obvious conceptual problem. How are these dynamical representations processed downstream of the retina? Some features, such as ones extracted by ON directional-selective cells and by melanopsin-containing ganglion cells, are transmitted to a variety of subcortical nuclei involved in specialized reflex pathways. A great number of features are analyzed by cortical circuits, so it is unlikely that the cortical units combine features extracted by the retina in a simple manner. This would essentially waste the effort put in by the retina in making up parallel channels. The divergence from retina to cortex — the fact that cortical visual areas, taken together, use a larger number of neurons and synapses to process retinal information and hence can deploy a higher computational power — also argues against such a scenario. For example, the four ON–OFF directional-selective cells, corresponding to the four compass directions, project to the lateral geniculate nucleus (LGN). Geniculate cells, in turn, relay information to primary or higher order visual cortices. This begs the question of how the four motion features follow their "processing route" within the cortex. A likely scenario, analogous to retinal processing, is that distinct features extracted by the retina interact with each other in cortex via inhibitory neurons. In this scheme, features are subtracted from each other, possibly according

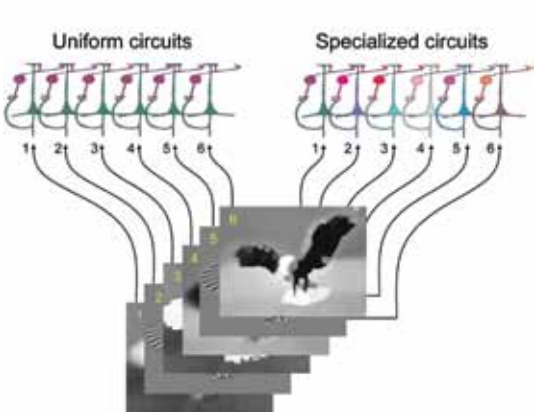


Figure 3. Parallel "retinal movies" from different ganglion cell types are relayed by the LGN to the visual cortex. These may couple to a uniform cortical circuitry (left). Alternatively, they may be processed by sets of specialized circuits (right).

to nonlinear computations, resulting in more sophisticated neuronal representations.

The logic and biological significance of feature recombination, as well as its interaction with orientation selectivity and other types of cortical selectivity, remain mysterious. A specific but central open question relates to the signals coming in from the LGN, driven by different types of retinal ganglion cells. Do these signals couple to a uniform cortical circuitry, or are they each routed through highly specific circuit paths (Fig. 3)? In both scenarios, features recombine; however, in the former, the "feature calculus" has regularities, while in the latter, it can take advantage of irregularities subject to feature-specific evolutionary and plastic refinements.

The retina can be pictured as a parallel assemblage comprising a multitude of small computational devices. Is the cortex to be viewed similarly as made up of intricately designed and specialized computational devices? Or are randomness, plasticity, and large-scale coupling the rules of the game? More specifically, how do local computations fit into the adaptive and plastic nature of cortical circuits, and are they compatible with the presence of strong feedback from remote areas and top-down control? Currently, there is no unified answer to this question. And indeed, the answer likely will depend on the specific cortical area and function. The methodologies highlighted above in the context of retina are opening a window onto the realm of the cortex.

It is customary to make parallels between a brain and a digital computer, in an effort to understand the former. For example, wiring cost is often invoked as a constraint that matters in the designs of both; accordingly, circuits ought to minimize total wire length. But brains and computers differ dramatically from one another, from both a functional and computational point of view. Biological processing units — neurons, or even subcellular units such as dendrites or synapses — are computationally sophisticated, specialized, and diverse. By contrast, digital computers are assembled from a few kinds of processing units, which are parallelized or serialized. Microcircuits in the brain capitalize on the richness of the basic machinery to yield a zoology of cell types. This ensures sophistication, specialization, and diversity on a higher computational plane and over broader temporal, spatial, and functional domains. The oft-quoted parallels between brain and computer may be overemphasizing the "hardware constraints" invoked to understand their makeup, when in reality, such constraints may be tempered by possibly more important requirements of function and computation.

## Acknowledgments

We are grateful to Michael J. Berry II for helpful discussions. This work was supported by the Centre National de la Recherche Scientifique through Unité Mixte de Recherche 8550 (RAdS) and by Friedrich Miescher Institute funds; a US Office of Naval Research Naval International Cooperative Program grant; and a National Center for Competence in Research Genetics grant, European Research Council grant, and RETICIRC, TREATRUSH, SEEBETTER, and OPTONEURO grants from the European Union to B.R.

NOTES

# Proteomic Studies of a Single CNS Synapse Type: The Parallel Fiber/ Purkinje Cell Synapse

Fekrije Selimi, PhD[1]; Ileana M. Cristea, PhD[2]; Elizabeth Heller, PhD[3]; Brian T. Chait, PhD[2]; and Nathaniel Heintz, PhD[3]

[1]Collège de France, Center for Interdisciplinary Research in Biology
Centre National de la Recherche Scientifique Unité Mixte de Recherche 7241
Institut National de la Santé et de la Recherche Médicale U1050
University Pierre and Marie Curie
MemoLife Laboratory of Excellence and Paris Sciences & Lettres
Paris, France

[2]Laboratory for Mass Spectrometry and Gaseous Ion Chemistry
The Rockefeller University
New York, New York

[3]Laboratory of Molecular Biology
Howard Hughes Medical Institute
The Rockefeller University
New York, New York

NOTES

## Introduction

Each of the thousands of cell types present in the nervous system receives multiple classes of inputs that are spatially segregated and functionally distinct. The chemoaffinity hypothesis stated in part that "the establishment and maintenance of synaptic associations were conceived to be regulated by highly specific cytochemical affinities" (Sperry, 1963). Support for this idea has come from studies of specific synaptic proteins (Benson et al., 2001) and from physiological studies of synaptic plasticity (Jorntell and Hansel, 2006). More than 1000 different postsynaptic proteins have been identified in "bulk" postsynaptic density preparations or in affinity-purified receptor complexes (Cho et al., 1992; Husi et al., 2000; Walikonis et al., 2000; Peng et al., 2004; Cheng et al., 2006; Collins et al., 2006). However, studies aimed at systematically identifying the protein composition of individual synapse types, and understanding their mechanistic diversity, have not been reported. To address this gap, we have developed synaptic protein profiling as an approach to isolate and biochemically characterize specific types of CNS synapses. We chose to first analyze the parallel fiber to Purkinje cell (PF/PC) synapse in the cerebellum because of its unique physiological properties and its involvement in neurological disease (Ito, 2001; Polleux and Lauder, 2004).

## Results

To enable purification of PF/PC synapses, we developed a transgenic mouse line that expresses an affinity tag only at the PF/PC synapse. We generated a fusion between the glutamate receptor delta2, GLURδ2, which is specifically localized at the PF/PC postsynaptic density (Yuzaki, 2003), and Venus, a variant of the green fluorescent protein (GFP). The resulting fusion protein, VGLURδ2, is properly processed and transported to the cell surface (data not shown). To express the fusion specifically in

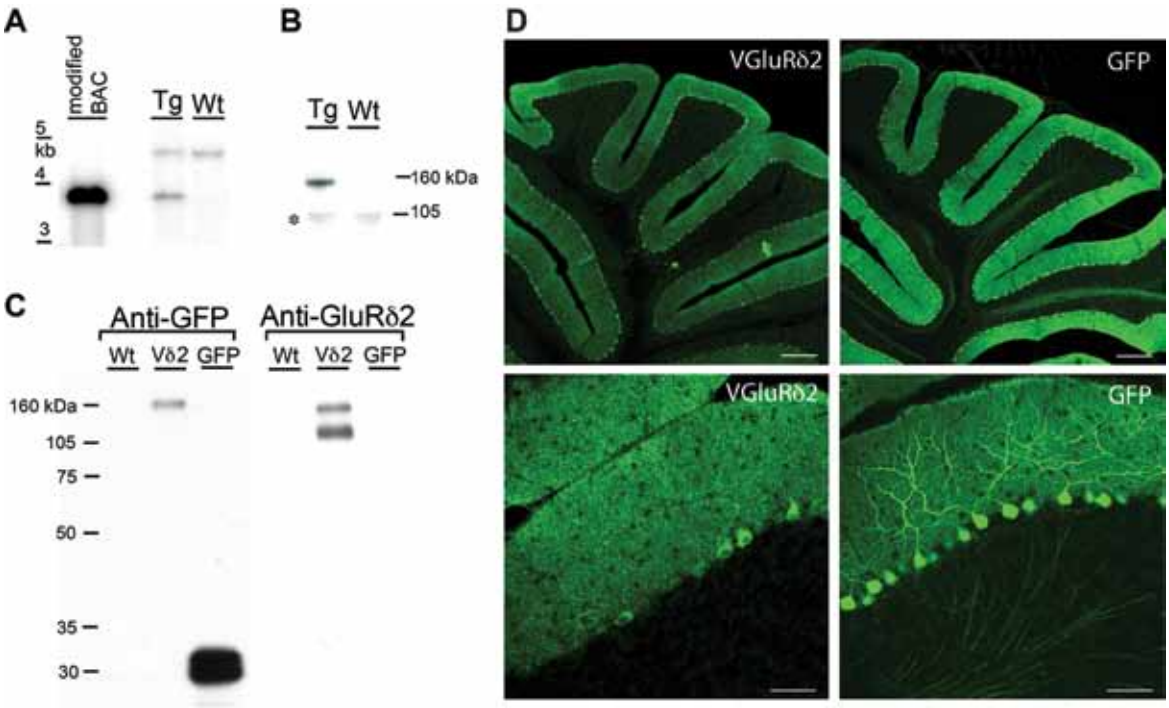


Figure 1. Tagging the PF/PC synapse in transgenic mice. ***A***, Southern blot was used to identify transgenic mice having integrated the *Pcp2* BAC (a Purkinje cell–specific driver) containing the Venus-tagged GLURδ2 receptor, VGLURδ2. ***B***, VGLURδ2 expression was detected using an anti-GFP antibody on immunoblots from total protein extracts of transgenic (Tg) versus wild-type (Wt) cerebella. * indicates a nonspecific band. ***C***, Both VGLURδ2 and GFP were affinity-purified using an anti-GFP antibody from 1% Triton X-100 cerebellar extracts from Wt, *Pcp2/VGluRδ2* (Vδ2), and *Pcp2/eGFP* control (GFP) mice, as shown by probing the immunoblots with an anti-GFP antibody (left). VGLURδ2 specifically copurified the endogenous GLURδ2, as shown by probing the same blot with an anti-GLURδ2 antibody (right). ***D***, Immunofluorescence on cerebellar sections using an anti-GFP antibody shows the specific localization of VGLURδ2 in the molecular layer and somata of Purkinje cells of Pcp2/VGluRδ2 mice. Soluble GFP is detected in the molecular layer, dendrites, somata, and axons of Purkinje cells in sections from Pcp2/eGFP mice. Scale bars: upper panels, 200 μm; lower panels, 50 μm.

NOTES

cerebellar Purkinje cells, the VGluRδ2 cDNA was then incorporated into a Pcp2 bacterial artificial chromosome (BAC) by homologous recombination, and the resulting *Pcp2/VGluRδ2* BAC construct was used to generate transgenic mice (Fig. 1*A*).

Expression of the fusion polypeptide was detected in the cerebellar extracts of *Pcp2/VGluRδ2* transgenic mice (Fig. 1*B*), and co-immunoprecipitation experiments demonstrated proper assembly of the VGLURδ2 fusion with the endogenous GLURδ2 receptor subunits (Fig. 1C). As shown in Figure *1D*, the localization of VGLURδ2 in the molecular layer and somata of PCs agrees with the synaptic localization of the GluRδ2 receptor. In contrast, the enhanced green fluorescent protein (eGFP) control protein expressed using the same BAC vector (Pcp2/eGFP) (www.gensat.org) is detected throughout the cell, including marked labeling of both Purkinje cell dendrites and axons (Fig. 1*D*).

Before the affinity purification step, we sought to produce cerebellar extracts enriched for synaptic structures relative to trafficking complexes, and to maximize the recovery of VGLURδ2-tagged postsynaptic densities (PSDs). This was performed by fractionating a solubilized crude synaptosome fraction (S3) on a gel-filtration column (Fig. 2*A*).

As shown in Figure 2*B* and 2C, this biochemical fractionation resulted in an enrichment of synaptic and mitochondrial proteins and a relative depletion of endoplasmic reticulum (ER) components in the high-molecular-weight fractions. These synaptic fractions contain essentially all of the PSD95 scaffolding protein. They also contain VGLURδ2, which was distributed among the different fractions in the same manner as wild-type GluRδ2 (Fig. 2C). This was also observed using standard synaptosome purification (data not shown) and shows that the fusion receptor VGLURδ2 is targeted to the synapse similarly to the wild-type GLURδ2.

To separate PF/PC postsynaptic densities from other cerebellar synapses, we performed affinity purification from the pooled synaptic fractions (red rectangle, Figure 2C) using an anti-eGFP antibody. Electron microscopy of the affinity-purified material showed

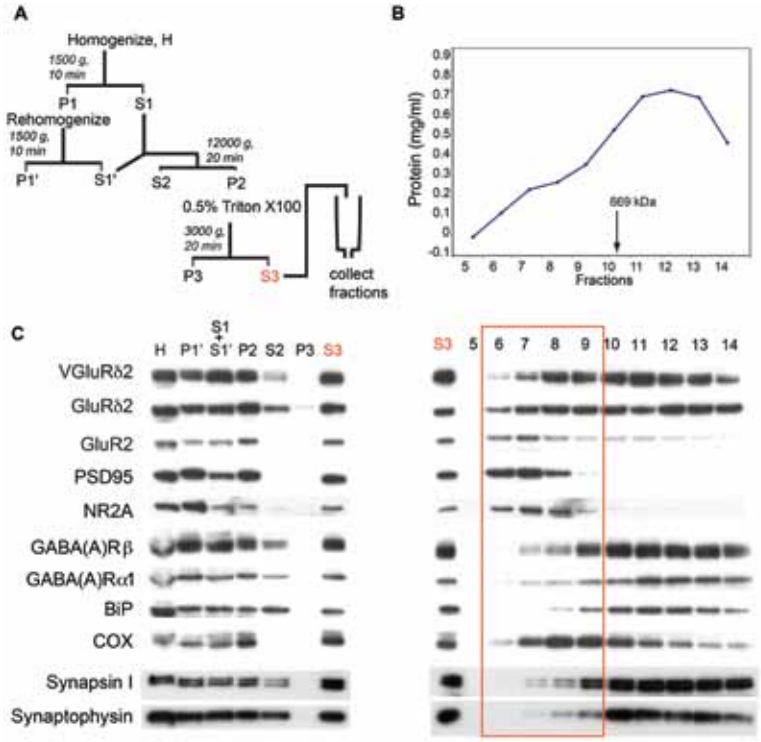


**Figure 2.** VGLURδ2 is detected in synaptic fractions using a new PSD purification method. ***A***, We prepared a crude synaptosome P2 fraction that was solubilized in 0.5% Triton X-100 final concentration. The extract was then separated on a Sephacryl S1000 gel filtration column (GE Healthcare, Uppsala, Sweden). ***B***, Protein dosage was performed on every fraction collected. ***C***, 0.1% in volume of every fraction was run on Western blots and assayed for the presence of excitatory synapse markers (GLURδ2, GLUR2/3, PSD95, NR2A), inhibitory synapse markers ($GABA_AR\beta$, $GABA_AR\alpha1$), the ER marker BiP, and the mitochondrial marker COX. VGLURδ2 was detected using an anti-GFP antibody. The red rectangle outlines the "synaptic" fractions enriched for synaptic markers and pooled for subsequent affinity purification of PF/PC PSDs.

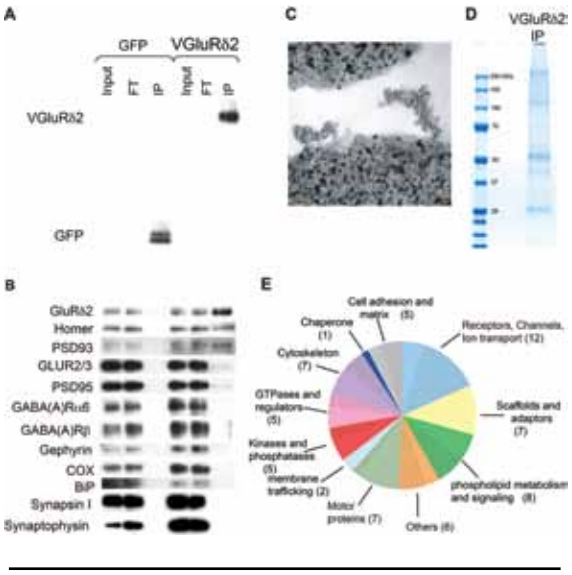


Figure 3. Affinity purification and protein profiling of the PF/PC PSDs. ***A***, Synaptic fractions from *Pcp2/VGluRδ2* animals were affinity-purified using magnetic beads coated with anti-GFP antibody (VGLURδ2). In parallel, control purifications were performed on preparations from *Pcp2/eGFP* transgenic mice (GFP). 0.025% of the inputs and flow-throughs (FT) and 25% of the affinity-purified samples (IP) were assayed by Western blot using an anti-GFP antibody and showed immunoprecipitation of both VGLURδ2 and GFP, respectively. ***B***, The same blot was probed for different synaptic markers and the mitochondrial protein COX, showing specific copurification of synaptic markers localized to the PF/PC synapse. ***C***, Electron microscopy shows the presence of electron-dense structures reminiscent of PSDs on the surface of the magnetic beads used for affinity purification of *Pcp2/VGluRδ2* extracts. ***D***, Mass spectrometry identified 65 different proteins in the complexes purified from *Pcp2/VGluRδ2* mice. ***E***, These proteins can be classified into 11 functional categories. The number of proteins from each category is indicated in parentheses. Nonshaded areas represent proteins found with high confidence.

electron-dense structures that were reminiscent of PSDs (Vinade et al., 2003) on the surface of the beads used for purification of VGLURδ2 extracts (Fig. 3C). These structures were absent from beads used to immunopurify extracts from *Pcp2/eGFP* control cerebella.

Using Western blot analysis, we were able to show that more than 50% of the target protein was immunopurified from the input extract for either the control eGFP or the VGLURδ2 extracts (Fig. 3A and data not shown). Western blotting also demonstrated copurification of several PF/PC synaptic components with VGLURδ2, including the GLURδ2 and GLUR2/3 receptors, and the scaffolding proteins PSD93 and Homer (Fig. 3*B*). Markers of inhibitory synapses ($GABA_A$ receptor α6, $GABA_A$ receptor β, and gephyrin) or of mitochondria (cytochrome oxidase [COX]) did not copurify, demonstrating the specificity of this approach (Fig. 3*B*). As expected, none of these markers copurified with soluble eGFP in extracts prepared from *Pcp2/eGFP* control mice (Fig. 3*B*). Taken together, these results demonstrate that the combination of cell-specific genetic targeting, molecular tagging of specific CNS synapses, biochemical fractionation, and affinity purification can be used to isolate a specific type of PSD from crude brain extracts.

To systematically identify components of the PF/PC PSDs, we analyzed the protein content of pooled PF/PC PSD preparations using single-stage and two-stage mass spectrometry (Cristea et al., 2005). A first experiment, using 30 *Pcp2/VGluRδ2* cerebella, enabled us to identify 12 components present at the PF/PC synapse but not present in the control sample, prepared in parallel from *Pcp2/eGFP* cerebella. To increase the number of PF/PC PSD components identified, we performed a second analysis on a sample prepared from 50 cerebella. A total of 65 proteins was identified: 37 proteins were detected with high confidence, and 28 were observed at lower levels and identified with less confidence. This analysis confirmed the presence of the PF/PC synapse proteins GLURδ2 (Yuzaki, 2003), Homer-3 (Shiraishi et al., 2004), PSD93 (Yuzaki, 2003), delphilin (Yuzaki, 2003), Shank1 and Shank2 (Uemura et al., 2004), and the absence of proteins located at other excitatory (NMDA receptor subunits, $GABA_A$ receptor α6) or inhibitory ($GABA_A$ receptor α6, $GABA_A$ receptor β, and gephyrin) synapses in the cerebellum. Forty of the identified proteins in our affinity-purified PSDs had been previously detected in preparations of synaptic proteins (Collins et al., 2006).

Approximately 700 different proteins have been identified in PSD preparations from whole brain (Collins et al., 2006). However, it has been estimated that, given several factors (the mass of a single PSD, the copy number of scaffold proteins in a PSD, and an average size of 100 kDa for each synaptic protein), only about 100 different proteins can be expected to be found at one particular type of PSD (Sheng and Hoogenraad, 2007). The number of proteins we found in this study was consistent with that estimate. Although it is probable that our analysis failed to identify all PF/PC postsynaptic proteins, the successful identification of AMPA receptor subunits in our preparations suggests that the proteins we failed to identify must be present at low stoichiometries in the PSD.

The 65 proteins we identified can be grouped into 11 different functional categories (Fig. 3*D*). These categories were previously annotated in studies of

NOTES

the PSD (Peng et al., 2004), with the exception of a class of proteins that we have called "phospholipid metabolism and signaling." In the "scaffolds and adaptors" category, several members of the Shank family (1 and 2) and the PSD family (PSD93 and PSD95) were detected at the PF/PC synapse, illustrating redundancy for scaffold proteins and underscoring their importance for synaptic function. Other functional categories included proteins important for synapse formation and physiology, such as regulators of small GTPases and protein kinases. Interestingly, eight of the proteins our study identified can regulate or be regulated by phospholipid metabolism (Iptr1, synaptojanin 1 and 2, phospholipase B, ABCA12, MRCKγ) or contain phospholipid-binding domains (Plekha7, annexin A6, MRCKγ). We therefore grouped them into a previously unrecognized category: "phospholipid metabolism and signaling." This suggests that phospholipid regulation is a major feature of the PF/PC synapse, in accordance with the major role that metabotropic glutamate receptor 1 (mGluR1) plays in regulating the physiology of the PF/PC synapse by activating phospholipase C (Ito, 2001; Jorntell and Hansel, 2006).

Another important category present at synapses groups receptors and ion channels: several glutamate receptor subunits and several G protein-coupled receptors ($GABA_B$ and BAI receptors) were detected in our analysis of the PF/PC PSD. Interestingly, the extracellular domain of BAI receptors contains thrombospondin repeats, which can mediate cell adhesion (Adams and Tucker, 2000). Several other proteins identified at the PF/PC synapse in our study are involved in cell adhesion and interaction with the extracellular matrix: receptor protein tyrosine phosphatases (Sallee et al., 2006), delta-catenin-2 (Kosik et al., 2005), Neph1 (Shen and Bargmann, 2003), and laminins (Dityatev and Schachner, 2006). The diversity of these potential recognition proteins at the PF/PC synapse shows the complexity of the "synaptic code" implied by the chemoaffinity hypothesis.

To provide additional evidence for the synaptic localization of the novel components that we have identified, we performed immunofluorescence studies on cerebellar sections from wild-type mice. Localization in the molecular layer of the cerebellum, which contains the PF/PC synapses, was evident for MRCKγ, Gm941, BAIAP2, RPTPm, Neph1, and δ2-catenin (Fig. 4). δ2-catenin and Gm941 could also be detected in some cerebellar

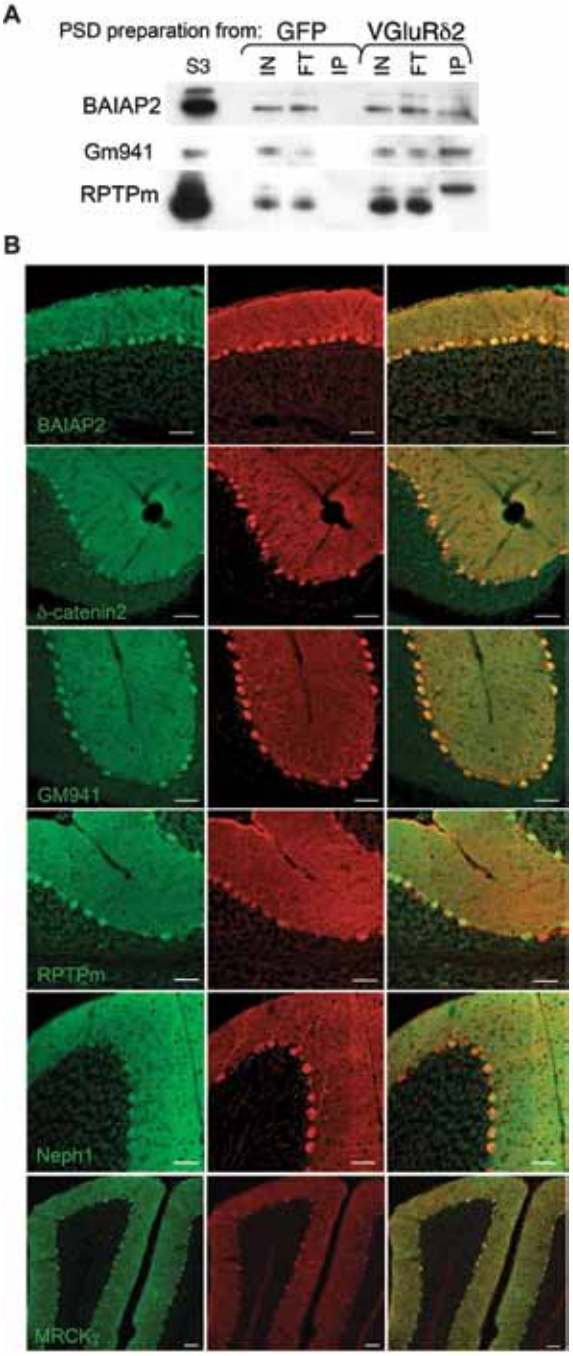


**Figure 4.** Localization of several candidate synaptic proteins at the PF/PC synapses. ***A***, Presence of selected candidates in PF/PC PSDs purified from *Pcp2/VGluRδ2* cerebella. 0.025% of the inputs (IN) and flow-throughs (FT) and 25% of the affinity-purified samples (IP) obtained from *Pcp2/eGFP* control (GFP) and *Pcp2/ VGluRδ2* (VGluRδ2) cerebella were assayed by Western blot. ***B***, Localization by immunofluorescence of candidate synaptic proteins. Labeling was performed using antibodies recognizing several candidate proteins identified by mass spectrometry (green) in conjunction with an anti-calbindin antibody specifically labeling Purkinje cells (red). Scale bars, 50 μm.

NOTES

interneurons. We also examined the expression of candidates reported in *in situ* hybridization databases (www.stjudebgem.org; www.brain-map.org; www.genepaint.org). Interpretable data were available for 36 candidates, and all but two were expressed in Purkinje cells, with a majority showing little detectable expression in the granule cell layer (data not shown). These expression data provide additional confirmation that the majority of the proteins our study identified are bona fide components of the PF/PC synapse.

## Discussion

The demonstration that the biochemical components of specific synapse types from a particular neuronal population can be identified using the approach described here has important implications. First, comparative synaptic protein profiling of different CNS synapse types using this strategy (combining specific synaptic tags and genetic targeting) can lead to a direct test of the chemoaffinity hypothesis (Sperry, 1963), as shown by the variety of potential recognition proteins found at the PF/PC synapse in this study. Second, synaptic protein profiling can reveal novel sets of proteins that allow us to formulate specific hypotheses regarding synaptic physiology. For example, the discovery of MRCKγ at PF/PC synapses has implications for the study of neurodevelopmental diseases, such as autism spectrum disorders and mental retardation. There is a frequent occurrence of Purkinje cell aplasia in autism (Polleux and Lauder, 2004) and a link between another small GTPase-dependent kinase, PAK3, and mental retardation (Allen et al., 1998). Third, our results suggest a complex regulatory role for phospholipids at postsynaptic densities, in addition to their important roles in regulating ion-channel permeability, and in vesicle trafficking at the presynaptic membrane (Di Paolo and De Camilli, 2006). We anticipate that further studies of biochemical diversity synapses will be critical for understanding the development and function of specific CNS circuits and their dysfunction in disease (Kennedy, 2000; Serajee et al., 2003).

## Acknowledgments

Parts of this paper have been published previously in *PLoS Biology* (2009;7:e1000083). Please refer to the published paper for additional materials and methods and supplemental figures and tables. We thank Professor Cornelia Bargmann and Dr. Anne Schaefer for a critical reading of the manuscript and helpful discussions. We also thank the Bioimaging facility at The Rockefeller University, in particular, Helen Shio for electron microscopy analysis and Alison North. We thank Kasia Losos for injection of transgenics and Jie Xing and Wendy Lee for technical assistance. We thank Dr. Myriam Heiman for help with the goat anti-GFP serum affinity-purification and Professor Chugh for the anti-Neph1 antibody. F.S. was supported by a fellowship from the Human Frontier Science Program Organization and I.M.C. by The Rockefeller University Women and Science Fellowship CEN5300379. This work was supported by grants from the Simons Foundation and National Institutes of Health grants RR00862 and RR02220 to B.T.C.

## References

Adams JC, Tucker RP (2000) The thrombospondin type 1 repeat (TSR) superfamily: diverse proteins with related roles in neuronal development. Dev Dyn 218:280-299.

Allen KM, Gleeson JG, Bagrodia S, Partington MW, MacMillan JC, Cerione RA, Mulley JC, Walsh CA (1998) *PAK3* mutation in nonsyndromic X-linked mental retardation. Nat Genet 20:25-30.

Benson DL, Colman DR, Huntley GW (2001) Molecules, maps and synapse specificity. Nat Rev Neurosci 2:899-909.

Cheng D, Hoogenraad CC, Rush J, Ramm E, Schlager MA, Duong DM, Xu P, Wijayawardana SR, Hanfelt J, Nakagawa T, Sheng M, Peng J (2006) Relative and absolute quantification of postsynaptic density proteome isolated from rat forebrain and cerebellum. Mol Cell Proteomics 5:1158-1170.

Cho KO, Hunt CA, Kennedy MB (1992) The rat brain postsynaptic density fraction contains a homolog of the drosophila discs-large tumor suppressor protein. Neuron 9:929-942.

Collins MO, Husi H, Yu L, Brandon JM, Anderson CN, Blackstock WP, Choudhary JS, Grant SG (2006) Molecular characterization and comparison of the components and multiprotein complexes in the postsynaptic proteome. J Neurochem 97 (Suppl 1):16-23.

Cristea IM, Williams R, Chait BT, Rout MP (2005) Fluorescent proteins as proteomic probes. Mol Cell Proteomics 4:1933-1941.

Di Paolo G, De Camilli P (2006) Phosphoinositides in cell regulation and membrane dynamics. Nature 443:651-657.

Dityatev A, Schachner M (2006) The extracellular matrix and synapses. Cell Tissue Res 326:647-654.

NOTES

Husi H, Ward MA, Choudhary JS, Blackstock WP, Grant SG (2000) Proteomic analysis of NMDA receptor-adhesion protein signaling complexes. Nat Neurosci 3:661-669.

Ito M (2001) Cerebellar long-term depression: characterization, signal transduction, and functional roles. Physiol Rev 81:1143-1195.

Jorntell H, Hansel C (2006) Synaptic memories upside down: bidirectional plasticity at cerebellar parallel fiber-Purkinje cell synapses. Neuron 52:227-238.

Kennedy MB (2000) Signal-processing machines at the postsynaptic density. Science 290:750-754.

Kosik KS, Donahue CP, Israely I, Liu X, Ochiishi T (2005) Delta-catenin at the synaptic-adherens junction. Trends Cell Biol 15:172-178.

Peng J, Kim MJ, Cheng D, Duong DM, Gygi SP, Sheng M (2004) Semiquantitative proteomic analysis of rat forebrain postsynaptic density fractions by mass spectrometry. J Biol Chem 279:21003-21011.

Polleux F, Lauder JM (2004) Toward a developmental neurobiology of autism. Ment Retard Dev Disabil Res Rev 10:303-317.

Sallee JL, Wittchen ES, Burridge K (2006) Regulation of cell adhesion by protein-tyrosine phosphatases: II. Cell-cell adhesion. J Biol Chem 281:16189-16192.

Serajee FJ, Nabi R, Zhong H, Mahbubul Huq AH (2003) Association of *INPP1, PIK3CG*, and *TSC2* gene variants with autistic disorder: implications for phosphatidylinositol signalling in autism. J Med Genet 40:e119.

Shen K, Bargmann CI (2003) The immunoglobulin superfamily protein SYG-1 determines the location of specific synapses in *C. elegans*. Cell 112:619-630.

Sheng M, Hoogenraad CC (2007) The postsynaptic architecture of excitatory synapses: a more quantitative view. Annu Rev Biochem 76:823-847.

Shiraishi Y, Mizutani A, Yuasa S, Mikoshiba K, Furuichi T (2004) Differential expression of Homer family proteins in the developing mouse brain. J Comp Neurol 473:582-599.

Sperry RW (1963) Chemoaffinity in the orderly growth of nerve fiber patterns and connections. Proc Natl Acad Sci USA 50:703-710.

Uemura T, Mori H, Mishina M (2004) Direct interaction of GluRδ2 with Shank scaffold proteins in cerebellar Purkinje cells. Mol Cell Neurosci 26:330-341.

Vinade L, Chang M, Schlief ML, Petersen JD, Reese TS, Tao-Cheng JH, Dosemeci A (2003) Affinity purification of PSD-95-containing postsynaptic complexes. J Neurochem 87:1255-1261.

Walikonis RS, Jensen ON, Mann M, Provance DW, Jr., Mercer JA, Kennedy MB (2000) Identification of proteins in the postsynaptic density fraction by mass spectrometry. J Neurosci 20:4069-4080.

Yuzaki M (2003) The delta2 glutamate receptor: 10 years later. Neurosci Res 46:11-22.

# Molecular Identification of Rapidly Adapting Mechanoreceptors and Their Developmental Dependence on Ret Signaling

Wenqin Luo, MD, PhD[1]; Hideki Enomoto, MD, PhD[2]; Frank L. Rice, PhD[3,4]; Jeffrey Milbrandt, MD, PhD[5]; and David D. Ginty, PhD[1]

[1]Solomon H. Snyder Department of Neuroscience
Howard Hughes Medical Institute
The Johns Hopkins University School of Medicine
Baltimore, Maryland

[2]Laboratory for Neuronal Differentiation and Regeneration
RIKEN Center for Developmental Biology
Kobe, Japan

[3]Center for Neuropharmacology and Neuroscience
Albany Medical College
Albany, New York

[4]Integrated Tissue Dynamics, LLC
Renssalaer, New York

[5]Department of Pathology
Washington University in St. Louis School of Medicine
St. Louis, Missouri

## Abstract

In mammals, the first step in the perception of form and texture is the activation of trigeminal or dorsal root ganglion (DRG) mechanosensory neurons, which are classified as either rapidly adapting (RA) or slowly adapting (SA) according to their rates of adaptation to sustained stimuli. The molecular identities and mechanisms of development of RA and SA mechanoreceptors are largely unknown. We found that the "early Ret+" DRG neurons are RA mechanoreceptors, which form Meissner corpuscles, Pacinian corpuscles, and longitudinal lanceolate endings. The central projections of these RA mechanoreceptors innervate layers III–V of the spinal cord and terminate within discrete subdomains of the dorsal column nuclei. Moreover, mice lacking Ret signaling components are devoid of Pacinian corpuscles and exhibit a dramatic disruption of RA mechanoreceptor projections to both the spinal cord and medulla. Thus, the early Ret+ neurons are RA mechanoreceptors, and Ret signaling is required for the assembly of neural circuits underlying touch perception.

## Acknowledgment

This paper was published in the journal *Neuron* (2009;64:841–856).

NOTES

# Regional Rescue of SCA1 Phenotypes by *14-3-3ε* Haploinsufficiency in Mice Underscores Complex Pathogenicity in Neurodegeneration

Paymaan Jafar-Nejad, MD[1,4]; Christopher S. Ward[1]; Ronald Richman, BS[3]; Harry T. Orr, PhD[5]; and Huda Y. Zoghbi, MD[1,2,3,4]

[1]Department of Molecular and Human Genetics
[2]Department of Neuroscience
[3]Howard Hughes Medical Institute
Baylor College of Medicine
Houston, Texas

[4]Jan and Dan Duncan Neurological Research Institute
Texas Children's Hospital
Houston, Texas

[5]Department of Laboratory Medicine and Pathology, Department of Biochemistry, and Institute of Human Genetics
University of Minnesota
Minneapolis, Minnesota

NOTES

## Introduction

Neurodegenerative "proteinopathies," such as Parkinson's, Alzheimer's, and Huntington's diseases, often involve disruptions of protein homeostasis resulting from altered protein interactions, functions, or degradation (Liu et al., 2002; Giorgini and Muchowski, 2005; Yamin et al., 2008). This disruption may be most readily appreciated in the polyglutamine diseases, a group that includes nine different conditions caused by an expansion of a translated CAG tract (polyQ) in distinct genes (Gatchel and Zoghbi, 2005). Early investigations sought to understand the toxicity mediated specifically by the polyQ peptides (Nagai et al., 1999), which do indeed exert widespread neuronal toxicity when expressed on their own. Research during the past decade, however, has demonstrated that other domains in the polyQ-containing proteins are necessary for the disease-specific patterns of neurodegeneration. For example, serine 13 and 16 are important for huntingtin pathogenesis (Gu et al., 2009), and mutations in caspase cleavage sites block nuclear localization and toxicity of polyQ-expanded huntingtin and androgen receptor (Ellerby et al., 1999, Graham et al., 2006). In the case of expanded Atxn1, either mutation of the nuclear localization signal (Klement et al., 1998), deletion of the AXH domain (de Chiara et al., 2005; Tsuda et al., 2005), or a serine-to-alanine substitution at residue 776 prevents the appearance of SCA1 phenotypes in mice (Emamian et al., 2003).

SCA1 usually causes onset of slowly progressive gait ataxia in midlife to late life, eventually impairing overall motor coordination and producing dysarthria, hypometric saccades, weight loss, respiratory dysfunction, and premature death (Zoghbi and Orr, 1995; Sriranjini et al., 2010). Cerebellar Purkinje cells are the first to be affected, which accounts for the presenting ataxia, but the pons and brainstem are also prominently involved. *Sca1* knock-in mice, which bear a CAG expansion of 154Q at the endogenous locus ($Sca1^{154Q/+}$) (Watase et al., 2002), recapitulate the features of human SCA1: from ataxia and motor dysfunction to weight loss, progressive Purkinje cell degeneration, and premature death (Watase et al., 2002). Using these mice, we have shown that the pathogenicity of mutant Atxn1 derives not from interactions with novel proteins but from alterations in its interactions with various native protein partners (Chen et al., 2003; Lam et al., 2006; Bowman et al., 2007; Lim et al., 2008). In particular, the toxicity of mutant Atxn1 derives from its incorporation into its large (1.5–3 MDa) native complexes: the S776A substitution, which does not exert toxicity, prevents mutant Atxn1 from incorporating into its large complexes (Emamian et al., 2003; Lam et al., 2006); also, displacing mutant Atxn1 from its large native complexes by overexpressing its paralogue, Atxn1-like, suppresses the phenotypes of the $Sca1^{154Q/+}$ mice (Bowman et al., 2007). These findings highlight the importance of Atxn1 large native complexes in SCA1 pathophysiology *in vivo*.

One group of protein interactors is of particular interest for pathogenesis studies: those whose interaction with Atxn1 requires phosphorylation at S776 and is enhanced by the expansion of the polyglutamine tract (Chen et al., 2003). The *14-3-3* proteins, among the first identified Atxn1 interactors, fall into this category. Widely expressed in eukaryotic cells (Takahashi, 2003), these proteins are highly conserved — from yeast to mammals (Aitken et al., 1992); they bind to phosphopeptide motifs in a variety of cellular proteins and can protect their target proteins from proteolysis and dephosphorylation (Muslin et al., 1996). Consistent with this function, we previously found that overexpression of *14-3-3ε* stabilizes Atxn1 in cells and increases the toxicity of Atxn1[82Q] in the fly model (Chen et al., 2003). We therefore hypothesized that removing one copy of *14-3-3* might mitigate the disease phenotype. To select a particular isoform of *14-3-3* for genetic interaction studies was not exactly straightforward: several of the seven *14-3-3* isoforms found in mammals (Tzivion and Avruch, 2002), including ε, ζ, η, β, and γ, interact with Atxn1 (Chen et al., 2003). The interaction of the ε and ζ isoforms with Atxn1 was identified primarily by immunoprecipitation of Atxn1[82Q], whereas the β and ε isoforms were the most frequently identified partners in a yeast two-hybrid screen for Atxn1 interactors (Chen et al., 2003). Sequence similarity among *14-3-3* isoforms suggests that some of them are probably functionally redundant (Aitken et al., 1992); thus, the effects of deleting one copy of one isoform might be masked by the presence of other isoforms. The fact that $14\text{-}3\text{-}3\varepsilon^{-/-}$ mice die at birth, however, indicates that this isoform has distinct, nonredundant functions (Toyo-oka et al., 2003). We therefore chose *14-3-3ε* (also known as Ywhae) to breed with the $Sca1^{154Q/+}$ mice.

To our surprise, we found that *14-3-3ε* haploinsufficiency strongly rescued motor phenotypes but not other aspects of SCA1 that appear unrelated to the cerebellum. This finding led us to investigate the biochemical correlation of such rescue to reveal region-specific differences in Atxn1 complexes. The findings from this study demonstrate that different pathogenic processes can take place in different vulnerable brain regions, highlighting the complexity of mechanisms underlying neurodegeneration in a single disorder.

NOTES

## Results

### Diminishing *14-3-3ε* rescues the SCA1 motor phenotype and cerebellar neuropathology

Atxn1 protein level was clearly reduced in crude cerebellar extracts from *14-3-3ε*$^{+/-}$ mice (Fig. 1A). We conclude that *14-3-3ε* stabilizes Atxn1 protein *in vivo* in mouse cerebellum. To determine whether *14-3-3ε* gene dosage affects the SCA1 phenotype, we crossed *14-3-3ε*$^{+/-}$ animals with the *Sca1*$^{154Q/+}$ mice and assessed their motor coordination on the accelerating rotarod at 7 weeks of age and their general motor function with the open-field activity (OFA) test at 20 weeks of age. The *Sca1*$^{154Q/+}$; *14-3-3ε*$^{+/+}$ animals (from here on referred to as *Sca1*$^{154Q/+}$ mice), as expected, showed significantly worse performance both on the rotarod and OFA than their wild-type (Wt) littermates ($p < 0.001$ and $p < 0.05$, respectively) (Fig. 1*B*,*C*). Removing one copy of *14-3-3ε* in *Sca1*$^{154Q/+}$ mice, however, rescued both rotarod and OFA phenotypes (Fig. 1*B*,*C*).

Would *14-3-3ε* haploinsufficiency noticeably affect the cerebellar neuropathology of *Sca1*$^{154Q/+}$ mice? Although Purkinje cell (PC) loss is prominent in human patients, in adult *Sca1*$^{154Q/+}$ mice only about 10% of PCs are lost; dendritic arborization is the most notable pathologic sign (Watase et al., 2002; Bowman et al., 2007). At 32–35 weeks of age, *14-3-3ε* haploinsufficiency rescued PC dendritic phenotype ($p < 0.005$) (Fig. 1*D*). The complexity of dendritic arbors and PC soma in the *Sca1*$^{154Q/+}$; *14-3-3ε*$^{+/-}$ mice, as examined by immunofluorescent confocal imaging, resembled that of Wt littermates (Fig. 1*E*), and there was no PC loss normally observed in adult *Sca1*$^{154Q/+}$ animals ($p < 0.0001$) (Fig. 1*E*,*F*). Reducing *14-3-3ε* thus completely rescued the ataxia and cerebellar pathology caused by polyglutamine-expanded Atxn1.

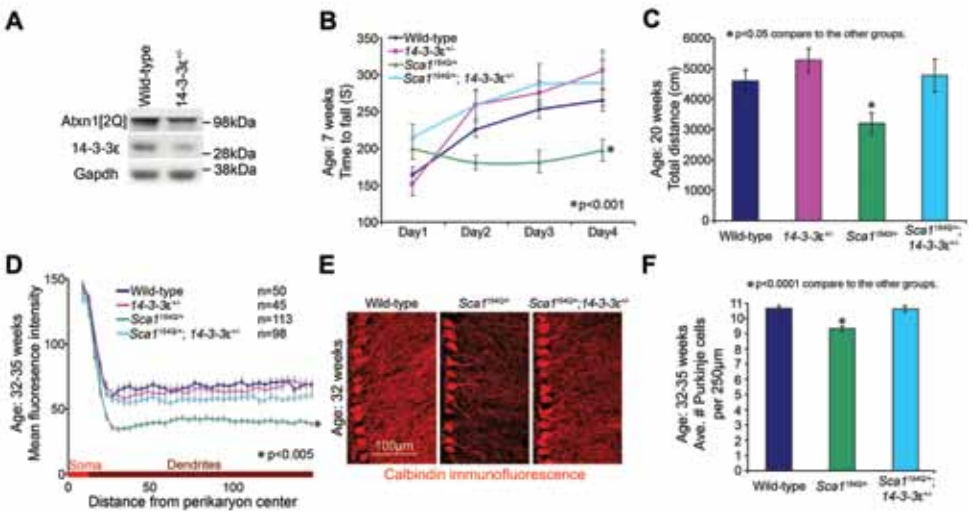


**Figure 1.** Haploinsufficiency of *14-3-3ε* rescues SCA1 cerebellar phenotype. ***A***, Western blot for *14-3-3ε*, Wt Ataxin1 (Atxn1[2Q]), and the control Gapdh in cerebellar lysates. ***B***, Accelerating rotarod; the average of 4 trials per day per animal (± SEM); (>19 animals/group); ANOVA; *14-3-3ε* haploinsufficiency rescues incoordination of *Sca1*$^{154Q/+}$ mice ($p < 0.001$) to Wt and *14-3-3ε*$^{+/-}$ littermates ($p = 0.27$ and $p = 0.47$, respectively). ***C***, OFA test; the average total distance traveled by each animal in 30 min (± SEM); (>19 animals/group); ANOVA; *14-3-3ε* heterozygosity restores activity level of *Sca1*$^{154Q/+}$mice to level of Wt or *14-3-3ε*$^{+/-}$ littermates ($p = 0.78$ and $p = 0.46$ respectively). ***D***, Quantitative calbindin immunofluorescence of cerebellar Purkinje cell dendrites. Mean fluorescence intensity of the indicated number of optical rectangular subsections from the crusI/II folia of 32- to 35-week-old animals ($n = 3$) was plotted as distance from perikaryon center (± SEM); ANOVA; *14-3-3ε* heterozygosity rescues the *Sca1*$^{154Q/+}$ loss of dendritic arborization phenotype ($p < 0.005$); there were no significant differences between double mutants and their Wt or *14-3-3ε*$^{+/-}$ littermates ($p = 0.18$ and $p = 0.47$, respectively). ***E***, Representative confocal images showing Purkinje cell morphology from the crusI/II folia of littermate-matched 32-week-old animals. Scale bar, 100 μm. ***F***, Quantification of Purkinje cell rescue, graphed as the average number of soma per 250 μm length (± SEM) along the Purkinje cell layer in individual confocal optical sections ($p < 0.0001$). (Wt: 807 neurons along 19,000 μm in $n = 18$ optical sections; *Sca1*$^{154Q/+}$: 867 neurons along 23,250 μm in $n = 23$ optical sections; *Sca1*$^{154Q/+}$; *14-3-3ε*$^{+/-}$: 858 neurons along 20,250 μm in $n = 20$ optical sections).

NOTES

## *14-3-3ε* haploinsufficiency reduces incorporation of mutant Atxn1 into its large native complexes

The pathogenicity of mutant Atxn1 correlates directly with its level: *Sca1*$^{154Q/154Q}$ and homozygote transgenic (B05) mice show significantly more severe phenotypes than their heterozygote littermates (Burright et al., 1995; Watase et al., 2002). Our *in vivo* data strongly suggest that the stability of the Wt Atxn1 depends, at least in part, on the presence of *14-3-3ε* at its physiological levels (Fig. 1A). *14-3-3ε* haploinsufficiency might therefore rescue the SCA1 cerebellar phenotypes by diminishing the levels of mutant Atxn1. Western blot analysis on crude cerebellar extracts showed that the *Sca1*$^{154Q/+}$; *14-3-3ε*$^{+/-}$ mice had significantly lower levels of both expanded Atxn1 and Wt Atxn1 compared with their *Sca1*$^{154Q/+}$ littermates (20% and 30%, respectively; $p < 0.05$) (Fig. 2*A–C*).

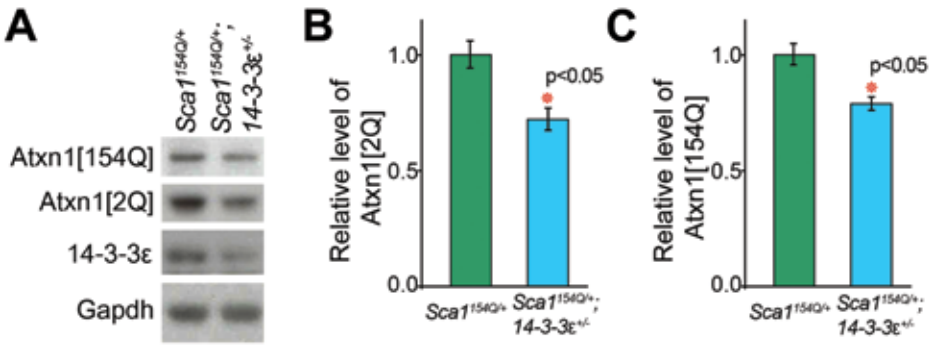


Figure 2. Haploinsufficiency of *14-3-3ε* decreases the levels of both Wt and expanded Ataxin1 in *Sca1*$^{154Q/+}$ mice. ***A–C***, Western blot analysis of mouse cerebellar extracts (genotypes indicated), using antisera to 14-3-3ε, Ataxin1 (2Q and 154Q), and Gapdh (control). The average level (±95% confidence interval) of Atxn1[2Q] and Atxn1[154Q] proteins in *Sca1*$^{154Q/+}$; *14-3-3ε*$^{+/-}$ relative to levels in *Sca1*$^{154Q/+}$ extracts is illustrated in panels ***B*** and ***C***, respectively ($n = 6$).

Given the importance of the Atxn1 large complexes in SCA1 pathogenesis, we next compared the formation of small and large Atxn1 complexes in *Sca1*$^{154Q/+}$; *14-3-3ε*$^{+/-}$ mice and their *Sca1*$^{154Q/+}$ littermates by analyzing the elution profiles of Atxn1[2Q] and Atxn1[154Q] in size-exclusion chromatography fractions of mouse cerebellar protein extracts (Fig. 3A). Quantification of the Atxn1 elution profiles showed that the ratio of large to small Atxn1[154Q] (but not Atxn1[2Q]) protein complexes in the *Sca1*$^{154Q/+}$; *14-3-3ε*$^{+/-}$ extracts was significantly lower than in the *Sca1*$^{154Q/+}$ extracts ($p = 0.011$) (Fig. 3*B–E*). These data suggest that, in addition to reducing Atxn1 levels, heterozygosity for *14-3-3ε* decreases the incorporation of Atxn1[154Q] into the large complexes, some of which are known to be toxic in the cerebellum.

## Heterozygosity for the *14-3-3ε* null allele does not rescue all SCA1 phenotypes

Despite the dramatic rescue of the motor phenotypes and cerebellar pathology, *14-3-3ε* haploinsufficiency did not mitigate the premature death or weight loss — phenotypes that are less likely to derive from cerebellar dysfunction (data not shown). In fact, the precise cause of death in *Sca1*$^{154Q/+}$ mice has never been established. Close observation of several *Sca1*$^{154Q/+}$ mice has shown that they are able to eat even a few hours before their death; postmortem studies of several *Sca1*$^{154Q/+}$ mice found food in the stomach and feces in the colon, so the animals do not starve to death. Aside from overall brain atrophy, however, we were unable to detect specific neuropathology in any other brain region than the cerebellum (Watase et al., 2002).

Patients with SCA1 suffer from pulmonary dysfunction that worsens over time and likely contributes to their death. Using spirometric tests, Sriranjini et al. (2010) found evidence of restrictive lung dysfunction, upper airway obstruction, and reduced muscle strength that could have arisen from a combination of factors, including pulmonary dormancy, poor respiratory muscle coordination, and bulbar dysfunction (Sriranjini et al., 2010). We therefore wondered if *Sca1*$^{154Q/+}$ mice, which replicate so many aspects of the human disease, might also suffer from respiratory dysregulation. Using unrestrained whole-body plethysmography, we assessed the basic respiratory pattern in *Sca1*$^{154Q/+}$ mice. At 5 weeks of age, the *Sca1*$^{154Q/+}$ mice did not differ significantly from their Wt littermates ($p = 0.16$); however, by 33 weeks of age, both *Sca1*$^{154Q/+}$ and *Sca1*$^{154Q/+}$; *14-3-3ε*$^{+/-}$ mice showed significantly more shallow,

NOTES

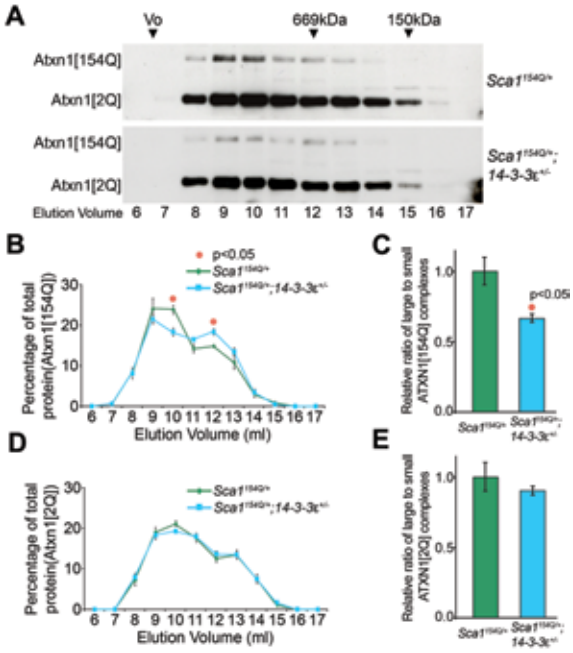


**Figure 3.** Haploinsufficiency of *14-3-3ε* shifts mutant Atxn1 from its large to its small complexes. ***A***, Representative Western blots of size exclusion chromatography fractions from mouse cerebellar extracts analyzed for Atxn1[2Q] and Atxn1[154Q]. The column void volume (Vo) and elution volume (ml) of each collected fraction are indicated. ***B***, The Atxn1[154Q] gel filtration elution profiles of cerebellar extract plotted as the percentage of Atxn1[154Q] (mean ± SEM) in each fraction (amount per fraction compared with total amount of Atxn1[154Q] in all fractions) from independent extracts. ***C***, Large (in the peak elution fractions, 9 and 10 ml) to small (in the peak elution fraction, 12 and 13 ml) Atxn1[154Q] complexes (mean ± SEM). ***D***, The Atxn1[2Q] gel filtration elution profiles of cerebellar extract plotted ($n$ = 4). ***E***, Large to small Atxn1[2Q] complexes (mean ± SEM) ($n$ = 4).

rapid respiration than their Wt littermates ($p < 0.01$) (data not shown). The respiratory phenotype of these mice, which has not been reported before, worsens with time, becoming most severe just prior to death. Suffice it to say, *14-3-3ε* haploinsufficiency does not appear to rescue phenotypes arising from parts of the nervous system outside of the cerebellum. The selective rescue of the SCA1 phenotypes in our genetic interaction raised the possibility of a distinct mechanism limited to the cerebellum.

## Atxn1 complex formation differs between the cerebellum and the brainstem

To investigate whether the biochemical changes we discovered are as specific to the cerebellum as the phenotypic rescue, we examined the brainstem. Not only is this brain region severely affected in SCA1, but bulbar dysfunction may well be involved in the nonrescued respiratory phenotype described above. To compare the biochemical studies on the brainstem with cerebellar findings, we had to answer two important questions: (1) whether *14-3-3ε* is expressed in the brainstem and (2) whether *14-3-3ε* and Atxn1 interact in the brainstem. Immunoblot analysis of cerebellar and brainstem lysates showed that *14-3-3ε* levels are the same in both regions (Fig. 4A). This is consistent with previous reports that *14-3-3ε* is ubiquitous in the brain (Baxter et al., 2002; Umahara et al., 2007). We then confirmed that Atxn1 co-immunoprecipitated with *14-3-3ε* in the brainstem (Fig. 4B). These results show that the reason for lack of rescue of a phenotype arising from the brainstem is neither lack of *14-3-3ε* expression nor lack of its interaction with Atxn1 in the brainstem.

A closer look at the protein levels in the extracts from the cerebellum and brainstem of *Sca1*$^{154Q/+}$ mice revealed that the level of Wt Atxn1 in the brainstem of the *Sca1*$^{154Q/+}$ mice was noticeably lower than in the cerebellum, but that the level of expanded Atxn1[154Q] was the same in both regions (Fig. 4A). The ratio of mutant to Wt Atxn1 in the brainstem was thus two to three times greater than in the cerebellum (Fig. 4C), which would likely make *14-3-3* heterozygosity less effective in mitigating brainstem degeneration.

We next quantified Atxn1 levels in crude brainstem extracts from the *Sca1*$^{154Q/+}$; *14-3-3ε*$^{+/-}$ mice and their *Sca1*$^{154Q/+}$ littermates. We found that, despite a decreased level of *14-3-3ε* in *Sca1*$^{154Q/+}$; *14-3-3ε*$^{+/-}$ mice, both Wt and mutant Atxn1 levels remained unaltered (data not shown).

Why does *14-3-3ε* haploinsufficiency fail to reduce Atxn1 levels in the brainstem of the *Sca1*$^{154Q/+}$; *14-3-3ε*$^{+/-}$ mice? The answer cannot involve regional differences in levels of either *14-3-3ε* or expanded Atxn1 (they are the same in both cerebellum and brainstem; Fig 4A) or lack of Atxn1/*14-3-3ε* interaction in the brainstem (Fig. 4B). We concluded that the mechanism by which *14-3-3ε* stabilizes Atxn1 must take place in the cerebellum but not in the brainstem. We analyzed the size-exclusion chromatography fractions of brainstem extracts from *Sca1*$^{154Q/+}$; *14-3-3ε*$^{+/-}$ mice and their *Sca1*$^{154Q/+}$ littermates. Unlike the cerebellum, the elution profiles of Atxn1[2Q] and Atxn1[154Q] in the brainstem of these two genotypes showed very similar patterns

NOTES

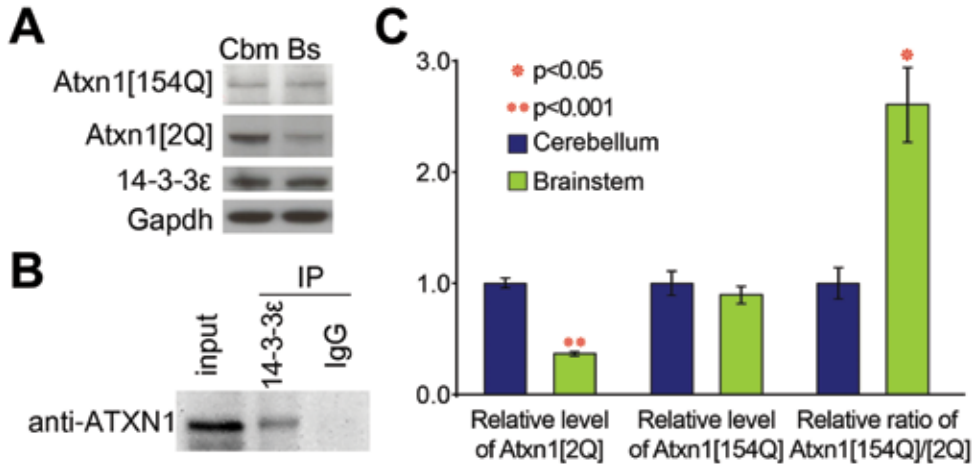


Figure 4. Level of Wt Atxn1, but not *14-3-3ε* and expanded Atxn1, is lower in the brainstem. ***A***, Western blot analysis of a *Sca1*$^{154Q/+}$ mouse cerebellar (Cbm) and brainstem (Bs) extracts, using antisera to *14-3-3ε*, Ataxin1 (2Q and 154Q), and Gapdh (control). ***B***, Co-immunoprecipitation of Atxn1 with *14-3-3ε* from Wt mouse brainstem extract. ***C***, The average levels of Atxn1[2Q] and Atxn1[154Q] proteins in *Sca1*$^{154Q/+}$; *14-3-3ε*$^{+/-}$ relative to levels in *Sca1*$^{154Q/+}$ extracts and relative level of ATXN[154Q] to Atxn1[2Q] in the cerebellum and brainstem are illustrated (±95% confidence interval) ($n$ = 6). IgG, immunoglobulin G.

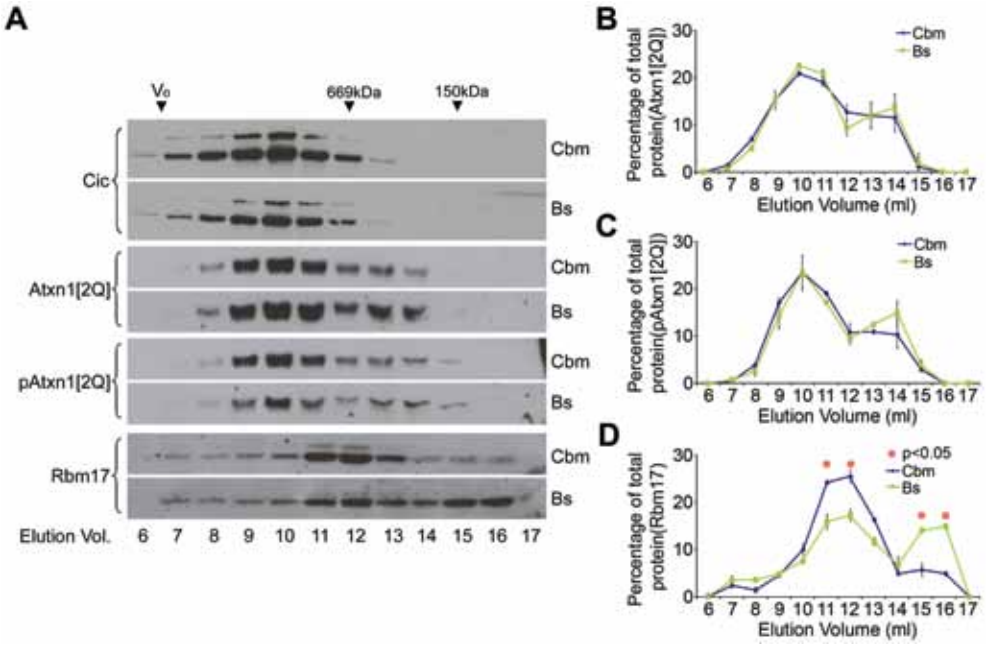


Figure 5. ***A***, Representative Western blots from size exclusion chromatography fractions of Wt mouse cerebellar (Cbm) and brainstem (Bs) extracts, analyzed for Capicua (Cic), Atxn1, pAtxn1, and Rbm17. The column void volume (Vo), size exclusion standards thyroglobulin (669 kDa) and alcohol dehydrogenase (150 kDa) and elution volume (ml) of each collected fraction are indicated. ***B***, The Atxn1[2Q] gel filtration elution profiles of cerebellar and brainstem extract from a Wt mouse plotted as the percentage of Atxn1[2Q] (mean ± SEM) in each fraction from independent extracts ($n$ = 3). ***C***, The pAtxn1[2Q] gel filtration elution profiles of cerebellar and brainstem extracts from a Wt mouse plotted as the percentage of pAtxn1[2Q] (mean ± SEM) in each fraction (amount per fraction compared with total amount of pAtxn1[2Q] in all fractions) from independent extracts ($n$ = 3). ***D***, The Rbm17 gel filtration elution profiles of cerebellar versus brainstem extracts from Wt mouse plotted as the percentage of Rbm17 (mean ± SEM) in each fraction (amount per fraction compared with total amount of Rbm17 in all fractions) from independent extracts ($n$ = 4).

NOTES

(data not shown); thus, *14-3-3ε* haploinsufficiency affected the elution profile of mutant Atxn1 in the cerebellum differently from the brainstem, suggesting that Atxn1 forms different native complexes in these two brain regions. To test this hypothesis, we analyzed the elution profiles of Atxn1, Capicua (a prominent native partner of Atxn1), and Rbm17 (a protein that interacts in an S776-dependent manner) (Lim et al., 2008) in size exclusion chromatography fractions of cerebellar and brainstem extracts from Wt mice. The elution profiles of total Atxn1, phospho-Atxn1 (pAtxn1), and Capicua were the same (Fig. 5*A*–*C*). The distribution of Rbm17 in the brainstem, however, differed from that in the cerebellum (Fig. 5*A*,*D*).

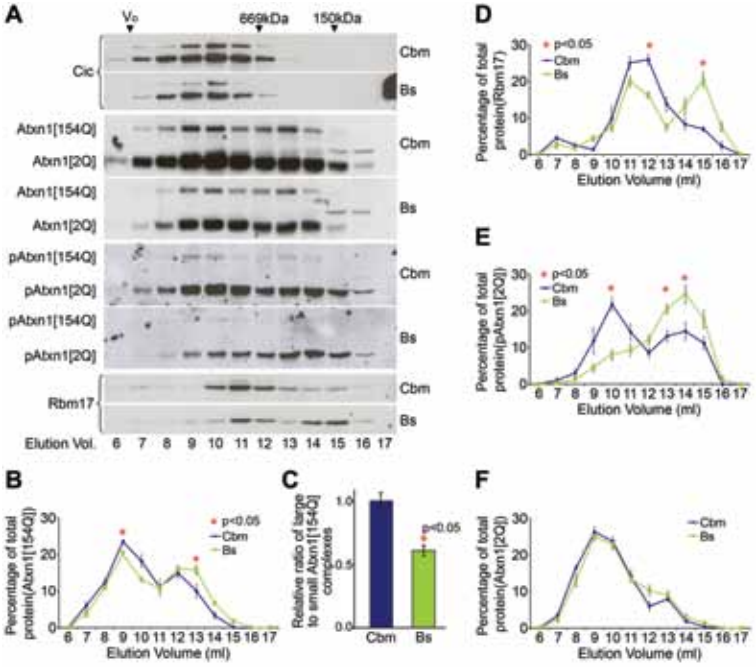


**Figure 6.** Brainstem (Bs) and cerebellum (Cbm) of *Sca1*$^{154Q/+}$ mice show different distributions of Atxn1[154Q], pAtxn1, and Rbm17. ***A***, Representative Western blots of size exclusion chromatography fractions from *Sca1*$^{154Q/+}$ cerebellar and brainstem extracts, analyzed for Capicua (Cic), Atxn1, pAtxn1, and Rbm17. ***B***, The Atxn1[154Q] gel filtration elution profiles of cerebellar and brainstem extracts from *Sca1*$^{154Q/+}$ plotted (mean ± SEM) ($n$ = 4). ***C***, Large to small Atxn1[154Q] complexes (mean ± SEM). Significantly less Atxn1[154Q] incorporated into the large complexes in the brainstem than in the cerebellum. Gel filtration elution profiles of ***D***, The Rbm17, ***E***, pAtxn1[2Q], and ***F***, Atxn1[2Q] from cerebellar and brainstem extracts from *Sca1*$^{154Q/+}$ plotted (mean ± SEM) ($n$ = 4).

In our *Sca1*$^{154Q/+}$mouse model, the elution profiles of Capicua and Atxn1[2Q] in the cerebellum and brainstem were similar to those of the Wt mice (Fig. 6*A*), but the ratio of large to small Atxn1[154Q] protein complexes was much lower ($p < 0.05$) in the brainstem than in the cerebellum (Fig. 6*A*–*C*). This suggests that expanded Atxn1 might have different partners that contribute to different toxic complexes in the two brain regions. In agreement with this notion, the elution profile of Rbm17 in *Sca1*$^{154Q/+}$ mice differed from the cerebellum to the brainstem (Fig. 6*A*,*D*).

Phosphorylation of Atxn1 at Serine 776 is critical for SCA1 pathogenesis (Chen et al., 2003; Emamian et al., 2003). The distribution of pAtxn1[2Q] and pAtxn1[154Q] in *Sca1*$^{154Q/+}$cerebellum followed the pattern of total Atxn1, with higher levels in large complexes than in the small ones (Fig. 6*A*). In *Sca1*$^{154Q/+}$ brainstem, however, the majority of endogenous, Wt pAtxn1 was found in small complexes, and very little was present in large Atxn1 complexes, even though they were enriched for total Atxn1[2Q] (Fig. 6*A*,*E*,*F*).

The very low levels of pAtxn1[154Q] in the brainstem prevented us from evaluating its elution profile (Fig. 6*A*). Given that the Wt brainstem and cerebellum showed no difference in the distribution of pAtxn1 (Fig. 5*A*,*C*), the lack of pAtxn1 in the large complexes in the brainstem of *Sca1*$^{154Q/+}$ mice must result from a specific effect of mutant Atxn1 in the brainstem. These data highlight major differences in the distribution pattern of mutant Atxn1 complexes in these two brain regions and suggest that pAtxn1 does not form the same complexes in the brainstem as it does in the cerebellum.

## Discussion

A growing body of literature is clarifying the mechanism of SCA1 pathogenesis in the cerebellum. The cerebellar symptoms in SCA1 are the first to appear and the easiest to measure, but the disease progresses to other serious symptoms that do not arise from the cerebellum. In the present study, we show that *14-3-3ε* haploinsufficiency in *Sca1*$^{154Q/+}$ mice rescues SCA1 cerebellar pathology and motor phenotypes. To our knowledge, this is the first dominant genetic suppressor to exhibit such a dramatic effect on the cerebellar phenotype in the *Sca1* mouse model. Our biochemical studies indicate that *14-3-3ε* stabilizes Atxn1; since the level of mutant Atxn1 directly correlates with its

NOTES

pathogenicity (Burright et al., 1995; Lorenzetti et al., 2000; Watase et al., 2002), it seems likely that the reduction in *14-3-3ε* alleviates cerebellar pathology at least in part by decreasing levels of mutant Atxn1.

We were surprised to find that *14-3-3ε* haploinsufficiency did not rescue all aspects of the phenotype, however: the double mutant mice still lost weight and died prematurely, just like their *Sca1*$^{154Q/+}$ littermates. Toyo-oka and colleagues showed that *14-3-3ε*$^{+/-}$ mice have mildly disorganized hippocampus and cortical thinning (Toyo-oka et al., 2003).These abnormalities, however, did not interfere with functions we assayed for in this study. We found that *14-3-3ε*$^{+/-}$ mice have normal motor coordination and Purkinje cell morphology, normal weight, breathing pattern, and lifespan. Hence, the mild cortical and hippocampal developmental defects in the *14-3-3ε*$^{+/-}$ mice are unlikely to be responsible for the nonrescued lifespan phenotype in *Sca1*$^{154Q/+}$; *14-3-3ε*$^{+/-}$ mice. In the course of trying to understand the cause of death, we uncovered a respiratory dysfunction that had not been reported previously in the *Sca1* knock-in mice but is documented in human patients (Sriranjini et al., 2010). While we were investigating this phenotype, four mice (two *Sca1*$^{154Q/+}$ and two *Sca1*$^{154Q/+}$; *14-3-3ε*$^{+/-}$ mice) died within two to four days of our last recording. Whether respiratory dysfunction was the immediate cause of death is impossible to ascertain; for that matter, the precise cause of death in human patients has not been firmly established. Aspiration pneumonia is a common (and frequently fatal) complication of end-stage SCA1 (Shiojiri et al., 1999; Ramio-Torrentia et al., 2006). This new unique, quantifiable phenotype in *Sca1*$^{154Q/+}$ mice could be used as an outcome measure in future studies of therapeutic interventions.

Notwithstanding the uncertain origins of the nonrescued phenotypes, we decided that examining Atxn1 complex formation in the brainstem, a brain region known to be highly vulnerable in SCA1, might provide insight into the apparently cerebellum-specific rescue. We found that, as previously reported (Baxter et al., 2002), *14-3-3ε* is expressed equally in the brainstem and in the cerebellum and that Atxn1 and *14-3-3ε* interact in both regions. The haploinsufficiency of *14-3-3ε*, however, decreased Ataxin1 levels only in the cerebellum; brainstem levels of both Wt and mutant Atxn1 were unaltered. In exploring the biochemical differences between the cerebellum and the brainstem, we found that some proteins (e.g., Rbm17) have completely different patterns in the two regions. In addition, the composition of the large Atxn1 complexes differs between the two regions: pAtxn1, which is necessary for *14-3-3*/Atxn1 interaction and for the toxicity of mutant Atxn1 in the large complexes in the cerebellum, is not present in the large Atxn1 complexes in the brainstem of *Sca1*$^{154Q/+}$ mice.

We also observed that the brainstem of *Sca1* mice has lower levels of Wt Atxn1 relative to the expanded protein. It is interesting to note in this context that previous work has shown Wt Atxn1 to exert a protective effect. We have postulated that Wt Atxn1 competes with mutant Atxn1 in binding some protein partners, and thereby reduces the formation of mutant Atxn1 complexes (Lim et al., 2008). The lower levels of Wt Atxn1 (and thus the greater availability of mutant Atxn1 for complex formation in the brainstem) could explain why genetic suppression by *14-3-3ε* heterozygosity is ineffective in the brainstem.

Selective neurodegeneration in the context of ubiquitous expression of the disease protein is a common feature of many neurodegenerative diseases (Orr and Zoghbi, 2007); it is a reasonable conjecture that differential vulnerability would be mediated by different protein interactions. What is striking in this study, however, is that we have examined two regions that are both targets of SCA1 and find evidence that pathogenesis in each region differs. In other words, the molecular pathogenesis of neuronal dysfunction within a single disorder can differ among affected brain regions. The finding that the distribution of the mutant protein in its native complexes can vary from one brain region to the next, and that such differences have region-specific effects, underscores the need for in-depth studies on molecular pathogenesis in the multiple cellular contexts typically affected by the disease, with a focus on native complexes. Our data also caution that potential therapeutic modalities should be examined in different brain regions and not generalized to the whole brain from one neuronal group.

## Acknowledgments

This paper was published in unabridged form in the journal *Proceedings of the National Academy of Sciences USA* (2011;108:2142-2147). Please refer to the published paper for further description of experimental procedures and supplementary figures. We are grateful to Dr. Anthony Wynshaw-Boris for providing *14-3-3ε*$^{+/-}$ mice; the assistance of the mouse phenotyping core facility at Baylor College of Medicine; Sukeshi Vaishnav for mouse genotyping; Dr. Hamed Jafar-Nejad, Dr. Herman Dierick,

NOTES

and the members of the H.Y.Z. laboratories for comments on the manuscript; and V.L. Brandt for editorial input. This work was supported by the National Institutes of Health Grant NS27699 to H.Y.Z., Grant NS022920 to H.T.O., and Grant HD024064 to the Baylor College of Medicine Intellectual and Developmental Disabilities Research Center.

## References

Aitken A, Collinge DB, van Heusden BP, Isobe T, Roseboom PH, Rosenfeld G, Soll J (1992) 14-3-3 proteins: a highly conserved, widespread family of eukaryotic proteins. Trends Biochem Sci 17:498-501.

Baxter HC, Liu WG, Forster JL, Aitken A, Fraser JR (2002) Immunolocalisation of 14-3-3 isoforms in normal and scrapie-infected murine brain. Neuroscience 109:5-14.

Bowman AB, Lam YC, Jafar-Nejad P, Chen HK, Richman R, Samaco RC, Fryer JD, Kahle JJ, Orr HT, Zoghbi HY (2007) Duplication of Atxn1l suppresses SCA1 neuropathology by decreasing incorporation of polyglutamine-expanded ataxin-1 into native complexes. Nat Genet 39:373-379.

Burright EN, Clark HB, Servadio A, Matilla T, Feddersen RM, Yunis WS, Duvick LA, Zoghbi HY, Orr HT (1995) *SCA1* transgenic mice: a model for neurodegeneration caused by an expanded CAG trinucleotide repeat. Cell 82:937-948.

Chen HK, Fernandez-Funez P, Acevedo SF, Lam YC, Kaytor MD, Fernandez MH, Aitken A, Skoulakis EM, Orr HT, Botas J, Zoghbi HY (2003) Interaction of Akt-phosphorylated ataxin-1 with 14-3-3 mediates neurodegeneration in spinocerebellar ataxia type 1. Cell 113:457-468.

de Chiara C, Menon RP, Dal Piaz F, Calder L, Pastore A (2005) Polyglutamine is not all: the functional role of the AXH domain in the ataxin-1 protein. J Mol Biol 354:883-893.

Ellerby LM, Hackam AS, Propp SS, Ellerby HM, Rabizadeh S, Cashman NR, Trifiro MA, Pinsky L, Wellington CL, Salvesen GS, Hayden MR, Bredesen DE (1999) Kennedy's disease: caspase cleavage of the androgen receptor is a crucial event in cytotoxicity. J Neurochem 72:185-195.

Emamian ES, Kaytor MD, Duvick LA, Zu T, Tousey SK, Zoghbi HY, Clark HB, Orr HT (2003) Serine 776 of ataxin-1 is critical for polyglutamine-induced disease in *SCA1* transgenic mice. Neuron 38:375-387.

Gatchel JR, Zoghbi HY (2005) Diseases of unstable repeat expansion: mechanisms and common principles. Nat Rev Genet 6:743-755.

Giorgini F, Muchowski PJ (2005) Connecting the dots in Huntington's disease with protein interaction networks. Genome Biol 6:210.

Graham RK, Deng Y, Slow EJ, Haigh B, Bissada N, Lu G, Pearson J, Shehadeh J, Bertram L, Murphy Z, Warby SC, Doty CN, Roy S, Wellington CL, Leavitt BR, Raymond LA, Nicholson DW, Hayden MR (2006) Cleavage at the caspase-6 site is required for neuronal dysfunction and degeneration due to mutant *huntingtin*. Cell 125:1179-1191.

Gu X, Greiner ER, Mishra R, Kodali R, Osmand A, Finkbeiner S, Steffan JS, Thompson LM, Wetzel R, Yang XW (2009) Serines 13 and 16 are critical determinants of full-length human mutant huntingtin induced disease pathogenesis in HD mice. Neuron 64:828-840.

Klement IA, Skinner PJ, Kaytor MD, Yi H, Hersch SM, Clark HB, Zoghbi HY, Orr HT (1998) Ataxin-1 nuclear localization and aggregation: role in polyglutamine-induced disease in *SCA1* transgenic mice. Cell 95:41-53.

Lam YC, Bowman AB, Jafar-Nejad P, Lim J, Richman R, Fryer JD, Hyun ED, Duvick LA, Orr HT, Botas J, Zoghbi HY (2006) ATAXIN-1 interacts with the repressor Capicua in its native complex to cause SCA1 neuropathology. Cell 127:1335-1347.

Lim J, Crespo-Barreto J, Jafar-Nejad P, Bowman AB, Richman R, Hill DE, Orr HT, Zoghbi HY (2008) Opposing effects of polyglutamine expansion on native protein complexes contribute to SCA1. Nature 452:713-718.

Liu Y, Fallon L, Lashuel HA, Liu Z, Lansbury PT, Jr. (2002) The *UCH-L1* gene encodes two opposing enzymatic activities that affect alpha-synuclein degradation and Parkinson's disease susceptibility. Cell 111:209-218.

Lorenzetti D, Watase K, Xu B, Matzuk MM, Orr HT, Zoghbi HY (2000) Repeat instability and motor incoordination in mice with a targeted expanded CAG repeat in the *Sca1* locus. Hum Mol Genet 9:779-785.

Muslin AJ, Tanner JW, Allen PM, Shaw AS (1996) Interaction of 14-3-3 with signaling proteins is mediated by the recognition of phosphoserine. Cell 84:889-897.

Nagai Y, Onodera O, Strittmatter WJ, Burke JR (1999) Polyglutamine domain proteins with expanded repeats bind neurofilament, altering the neurofilament network. Ann NY Acad Sci 893:192-202.

Orr HT, Zoghbi HY (2007) Trinucleotide repeat disorders. Annu Rev Neurosci 30:575-621.

Ramio-Torrentia L, Gomez E, Genis D (2006) Swallowing in degenerative ataxias. J Neurol 253:875-881.

Shiojiri T, Tsunemi T, Matsunaga T, Sasaki H, Yabe I, Tashiro K, Nishizawa N, Takamoto K, Yokota T, Mizusawa H (1999) Vocal cord abductor paralysis in spinocerebellar ataxia type 1. J Neurol Neurosurg Psychiatry 67:695.

Sriranjini SJ, Pal PK, Krishna N, Sathyaprabha TN (2010) Subclinical pulmonary dysfunction in spinocerebellar ataxias 1, 2 and 3. Acta Neurol Scand 122:323-328.

Takahashi Y (2003) The 14-3-3 proteins: gene, gene expression, and function. Neurochem Res 28:1265-1273.

Toyo-oka K, Shionoya A, Gambello MJ, Cardoso C, Leventer R, Ward HL, Ayala R, Tsai LH, Dobyns W, Ledbetter D, Hirotsune S, Wynshaw-Boris A (2003) 14-3-3ε is important for neuronal migration by binding to NUDEL: a molecular explanation for Miller-Dieker syndrome. Nat Genet 34:274-285.

Tsuda H, Jafar-Nejad H, Patel AJ, Sun Y, Chen HK, Rose MF, Venken KJ, Botas J, Orr HT, Bellen HJ, Zoghbi HY (2005) The AXH domain of Ataxin-1 mediates neurodegeneration through its interaction with Gfi-1/Senseless proteins. Cell 122:633-644.

Tzivion G, Avruch J (2002) 14-3-3 proteins: active cofactors in cellular regulation by serine/threonine phosphorylation. J Biol Chem 277:3061-3064.

Umahara T, Uchihara T, Yagishita S, Nakamura A, Tsuchiya K, Iwamoto T (2007) Intranuclear immunolocalization of 14-3-3 protein isoforms in brains with spinocerebellar ataxia type 1. Neurosci Lett 414:130-135.

Watase K, Weeber EJ, Xu B, Antalffy B, Yuva-Paylor L, Hashimoto K, Kano M, Atkinson R, Sun Y, Armstrong DL, Sweatt JD, Orr HT, Paylor R, Zoghbi HY (2002) A long CAG repeat in the mouse *Sca1* locus replicates SCA1 features and reveals the impact of protein solubility on selective neurodegeneration. Neuron 34:905-919.

Yamin G, Ono K, Inayathullah M, Teplow DB (2008) Amyloid beta-protein assembly as a therapeutic target of Alzheimer's disease. Curr Pharm Des 14:3231-3246.

Zoghbi HY, Orr HT (1995) Spinocerebellar ataxia type 1. Semin Cell Biol 6:29-35.

NOTES

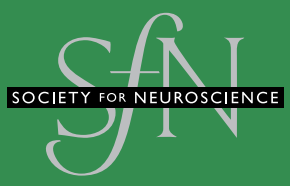


1121 14th Street, NW | Suite 1010 | Washington, DC 20005 | (202) 962-4000 | www.sfn.org